REVIEWS

Journal of Semiconductors
(2020) 41, 081002
doi: 10.1088/1674-4926/41/8/081002

Tellurene: An elemental 2D monolayer material beyond its bulk phases without van der Waals layered structures

Xiaolin Cai[1, 2, 4], Xiaoyu Han[3], Chunxiang Zhao[4], Chunyao Niu[4], and Yu Jia[2, 4, †]

[1]School of Physics and Electronic Information Engineering, Henan Polytechnic University, Jiaozuo 454000, China

[2]MOE Key Laboratory for Special Functional Materials and School of Materials Science and Engineering, Henan University, Kaifeng 475004, China

[3]Department of Chemistry, University of Manchester, Manchester M13 9PL, UK

[4]International Laboratory for Quantum Functional Materials of Henan and School of Physics and Microelectronics, Zhengzhou University, Zhengzhou 450001, China

Abstract: Due to the quantum confinement effect, atomically thin two-dimensional (2D) monolayer materials possess distinct characteristics from their corresponding bulk materials, which have received wide attention from science and industry. Among all the 2D materials, elemental 2D materials with the simplest components are most striking. As an emerging group-VIA elemental 2D monolayer material, tellurene exhibits many exciting fundamental properties, such as chemical and mechanical stabilities, bandgap and high carrier mobilities compared to phosphorene, graphene and MoS_2, respectively. Besides, in further exploration, it was found that tellurene or tellurene-based device presents excellent thermoelectric properties, piezoelectric properties, quantum Hall effects, and superb optical properties especially nonlinear optics characteristics, etc. The properties of tellurene can be modulated by virtue of strain, defects, edges, and heterojunction effects. In view of so many unique properties, it has drawn significant interest since tellurene was predicted and fabricated successfully in 2017. In this paper, we review the 2D tellurene allotropes, experimental preparation, excellent properties, performance modulation and future development.

Key words: tellurene; helical chain; anisortropy; phase transformation

Citation: X L Cai, X Y Han, C X Zhao, C Y Niu, and Y Jia, Tellurene: An elemental 2D monolayer material beyond its bulk phases without van der Waals layered structures[J]. *J. Semicond.*, 2020, 41(8), 081002. http://doi.org/10.1088/1674-4926/41/8/081002

1. Overview of elemental two-dimensional materials

Two-dimensional (2D) materials with atomic thickness demonstrate unique physical, chemical and mechanical characteristics against the corresponding three-dimensional (3D) forms. They could also be further modified by other means, such as nanostructuring, doping, twisting, etc. These provide new potential in the applicants of electronics, optoelectronics and energy storage devices, superconductors, etc. Hence, the research on 2D materials experienced an explosive growth since the pioneering work on graphene[1]. Up to now, a large number of 2D materials have been discovered and fabricated, which could be classified into two categories according to their structures. The first category, represented by graphene and h-BN monolayers (MLs), has six membered honeycomb-like structure. The other category is composed of triatomic layers, represented by transition metal disulfides (TMDs), metal halides (PbI_2, $MgBr_2$), transition metal carbon/nitrogen compounds (MXenes), elemental 2D materials (Xenes) other than graphene. Besides of their unique properties, those Xenes also have extended the allotropes of each element.

To our best knowledge, 15 types of elemental 2D materials in main group have been experimentally realized or theoretically predicted. They include borophene[2], aluminene[3], gallenene[4] and indiene[5] in IIIA group, graphene, silicene[6], germanene[7], stanene[8] and plumbene[9] in IVA group, phosphorene[10], arsenene, antimonene and bismuthene in VA group[11–13], and selenene and tellurene in VIA group[14], shown in Fig. 1(a). Except the aluminene and indiene only exist theoretically prediction, all the other 13 elemental 2D forms all have been successfully synthetized or fabricated. Fig. 1(b) depicts the timeline of the discovery of the 15 elemental 2D materials. Their intriguing and useful applications are summarized in Fig. 1(a)[15].

Tellurene is the 2D form of tellurium in group-VIA, which was proposed by theoretical calculations and then verified by experiments in 2017. Unlike other 2D MLs, such as graphene, tellurene has no layered counterparts. Its formation mechanism is the strain caused by competition between its multivalency and helical chain in the low-dimensional case. Tellurene has favourable properties such as high carrier mobility, excellent light absorption, superb thermoelectric performance and good stability at room temperature, which has great potential in nanodevices. Thus tellurene has aroused intensive attention since its advent. This review aims to summarize the latest progress and research status on tellurene. The review has been organized into five sections as follows. In the first section, the 2D material family as a whole is briefly discussed. In the second section, we review the theoretical prediction and experimental synthesis of tellurene. The excellent properties of tellurene are summarized in the third section.

Correspondence to: Y Jia, jiayu@zzu.edu.cn
Received 14 JUNE 2020; Revised 12 JULY 2020.

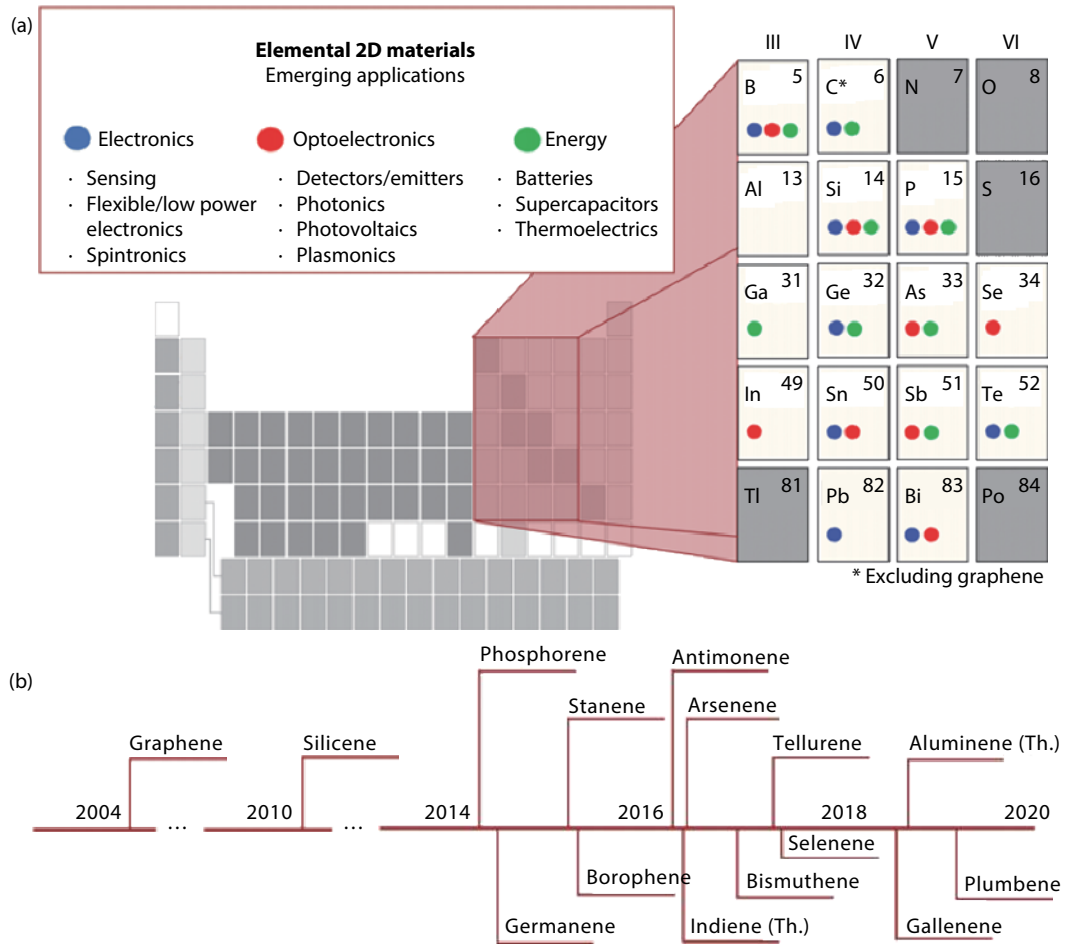

Fig. 1. (Color online) (a) Overview of 2D elemental main group materials and (b) the corresponding timeline of experimental realization, where "Th." represents only theoretical prediction[15].

The fourth section presents the performance modulation of tellurene as well as its functionalization. In the last section, we make some prospects to the future development of tellurene.

2. Rise of tellurene

Since the elemental 2D MLs in group-IIIA, -IVA and -VA have been developed, scientists began to challenge the possibility of group-VIA single element forming 2D atomic crystals. Structurally, the bulk structures of group-VIA are mostly chain-like, not the van der Waals (vdW) layered structure like graphite. Chemically, for the group-VIA elements (S, Se, Te), the difference of the absolute value of their oxidation states (+6 and –2) is larger than those in group-IIIA, -IVA and -VA. So, the existence of group-VIA 2D elemental MLs is a scientifically interesting and challenging issue. 3D is the source and foundation of 2D, and thus we firstly trace back to the crystal structure of 3D Te bulk together with its typical characteristics.

2.1. Te in bulk phase

In group-VIA, the nonmetallic element Te is located between the nonmetallic element Se and the metal element Po, which determines the metalloid property of Te. The most stable structure of Te at the room pressure is a trigonal one termed as Te-I, consisting of helical chains parallel to the *c*-axis, which run along the *c*-axis and are arranged in a hexagonal form. In the helical chain, each one third of atoms are straightly above other atoms, so that the projected plane of the chain forms an equilateral triangle (see Fig. 2(a)). Intrachain Te atoms are bound by covalent bonds through a helical turn of 120° in [0001] direction while interchain atoms are noncovalently bonded[16]. The valence electron configuration of Te atom is $5s^25p^4$. Due to the large s–p separation, its s electrons are considered to be in a core state. Covalent bonds are formed between two p electrons and their adjacent Te atoms in the chain, and a lone pair of electrons are composed of the left two p electrons allocating between the chains. Thus, the interchain interaction is weaker than the intrachain one[17].

Te-I is a semiconductor with the bandgap of 0.35 eV[18]. The effective Hamiltonians of Te-I had been constructed about half a century ago[19–25], which are performed to analyze the electronic property and symmetry, providing an important theoretical fundamental for further understanding tellurium. In the band structure of Te-I, the valence band maximum (VBM) is located at the vicinity of the H point, while the conduced band maximum (CBM) is at the H point, in which the band splitting of VBM and CBM near H point occurs due to the SOC effect[26] (see Fig. 2(e)). This unique band structure, such as the nested valence bands at the H point in the Brillouin zone, determines the excellent physical properties of Te-I. For instance, Te-I presents a high thermoelectric figure of merit of unity, which not only demonstrates the concept but also fills up the high performance gap from 300 to 700K

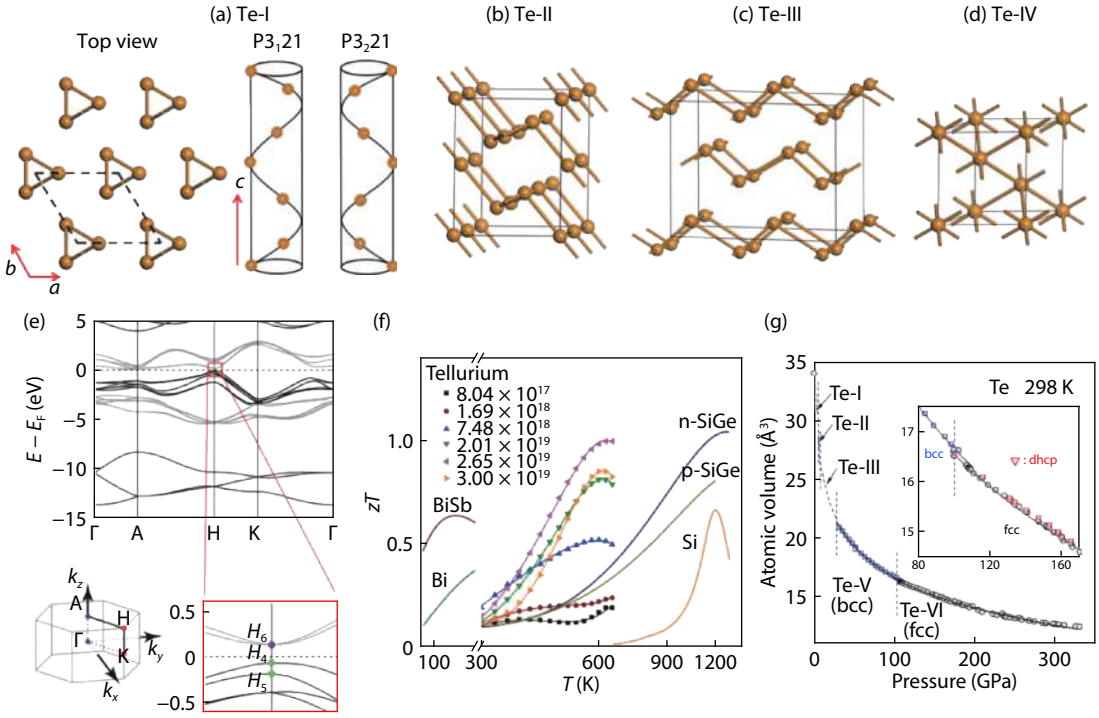

Fig. 2. (Color online) (a) Top view of crystal structure of Te-I as well as its helical chains of Te atoms run in righ- and left-hand manners. (b–d) different crystal structures of Te bulk under high pressure. (e) Band structures of Te-I[26]. (f) Figure of merit (zT) as a function of temperature for p-type ploycrystalline tellurium with different carrier concentrations[27]. (g) Pressure induced phase transition within 0 and 330 GPa[28].

for elemental thermoelectrics[27] (see Fig. 2(f)).

Like natural organic substances such as sugar, the Te-I bulk with the helical structure is a chiral crystal due to lack of mirror symmetry and inversion center, which has the inequivalent right- and left-handed structures with the space groups of $P3_121$ and $P3_221$ (see Fig. 2(a)), respectively. The chiral tellurium is suitable for engineering owing to the simplest crystal structure, which has received particular attention[26, 29–33]. The handedness of chiral Te crystals can be determined experimentally[29, 33]. Employing ab-initio electronic structure calculations, it was revealed that the Te-I can undergo the transition from trivial insulator to strong topological insulator (metal) under shear (hydrostatic or uniaxial) strain, which could be attributed to the depopulation of the lone-pair orbitals related to the valence band via proper strain engineering[26]. This result means that the trigonal Te is the prototype of a novel family of chiral-based 3D topological insulators, which has important applications in spintronics, magneto-optics, and thermoelectrics. Further, it was found that the Te-I has multiple Weyl nodes near the Fermi level, in which a hedgehog spin texture is formed near the H points[30]. Band splitting and Weyl nodes in the Te-I as well as its radial spin texture were investigated by angle-resolved photoemission spectroscopy[31, 32]. It was definitively evidenced that the band splitting and Weyl nodes in Te-I originate from its chirality of crystal through the band-structure mapping in the 3D Brillouin zone[31]. Moreover, a spin component of the highest valence band is parallel to the electron momentum around the Brillouin zone corners, and the spin polarization is reversed in the crystal with the opposite chirality[32], which indicates the hedgehoglike spin textures of the right- and left-handed chiral crystals, resulting in some unconventional magnetoelectric effects and nonreciprocal phenomena.

The bulk Te also has diverse phases under high pressure[34–38] (see Figs. 2(b), 2(c), and 2(d)), whose coordination numbers (CN) range from 2 to 12. When the pressure changes from 0 to 300 GPa, there mainly exist five phases except for trigonal Te-I phase in the Te bulk, shown in Fig. 2(g). They are the Te-II phase of a monoclinic structure with the CN of 4 (see Fig. 2(b)), the Te-III phase of an orthogonal structure with the CN of 4 (see Fig. 2(c)), the Te-IV phase of the β-Po structure with the CN of 6 (see Fig. 2(d)), the Te-V phase of the body centered-cubic structure with the CN of 8, and the Te-VI phase of the body centred-cubic with the CN of 12, respectively.

2.2. Advent of 2D tellurene

By combining the particle-swarm optimization searches[39] with density functional theory (DFT) calculations, Zhu *et al.* predicted that the group-VIA Te can form stable ML, named tellurene. Te has the inherent multivalency, which competes with the chain structure in the low dimensional case leading to large strain. These factors drive Te to form stable ML structure. It was revealed that 2D ML tellurene can exist in three structures, namely the most stable 1T-MoS_2-like (α-Te) structure, together with the metastable tetragonal (β-Te) and 2H-MoS_2-like (γ-Te) structures (See Fig. 3). α-Te and β-Te are semiconductors possessing the bandgaps of 0.75 and 1.47 eV, respectively, in which the carrier mobilities are up to 10^3 $cm^2V^{-1}s^{-1}$, higher than that of MoS_2. And the optical absorptions are more than 10^5 cm^{-1}. Intriguingly, β-Te exhibits anisotropy in electronic and optical properties. The superb photoelectric properties make tellurene promising in optoelectronic devices, valleytronics and photon detection. Furthermore, Zhu *et al.* also provided preliminary but convincing experimental evidence on the layering property of Te on highly oriented pyrolytic graphite (HOPG) substrates, and

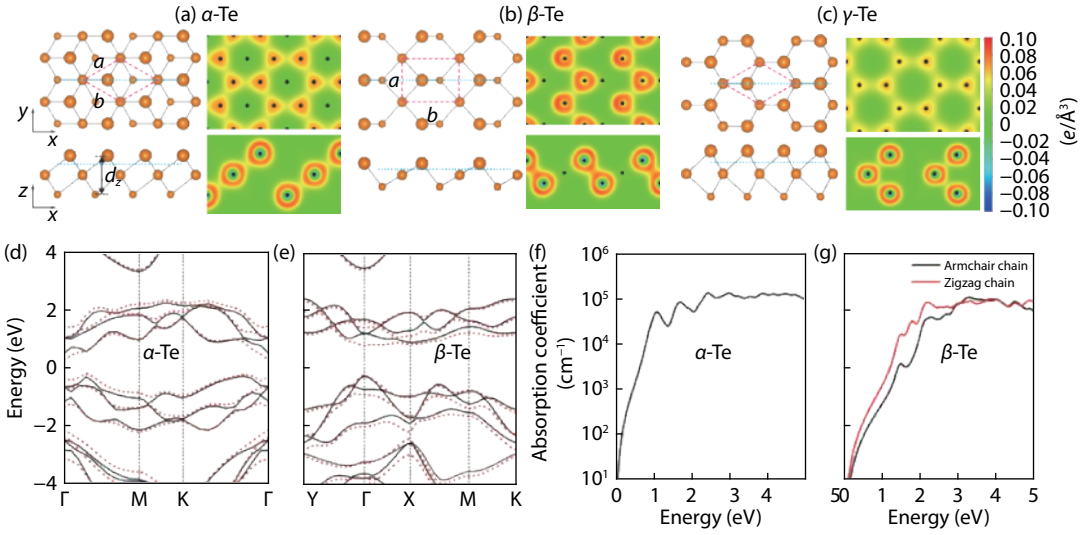

Fig. 3. (Color online) Crystal structures and total charge densities of three kinds of tellurene, as well as the electronic band structure and optical absorption of α-Te and β-Te[11].

pointed out the important role of multivalency in the layering property of Se. Their findings firstly expanded 2D elemental ML materials to group-VIA, and provided new ideas for the design of 2D materials[14]. Later, Professor Reed in Stanford University highlighted these Te research results in the column of News & Views of Nature magazine, and said that the fact that the potential existence of 2D tellurene was revealed by computational simulations, reflects a crucial role of computational approaches played in addressing important problems of materials science[40].

The theoretical work on the group-VIA 2D ML tellurene published attracted wide interest of scholars. Now, it has been four years since the firstly submitted 2D tellurene manuscript on arXiv platform in January 2016, and there have been a great many studies on the experimental preparation, property study and application exploration of tellurene. Herein, we will review these studies, hoping to introduce newcomers to the field of tellurene and stimulating their interest.

2.3. Prediction of multiple 2D tellurene structures

In view of the multivalency induced diverse phases of bulk Te under high-pressure[14, 41], it is believed that the structure of 2D Te may have more besides the above proposed three phases of 2D tellurene.

By artificially compressing a 2D assembly of the native helices in the normal direction of the 2D layer, Liu *et al.* obtained abnormally stable 2D δ-Te as well as δ-Se. And the stable η-phase is obtained by a series of reflections of δ-structure with fixing the bond lengths and bond angles constant. δ- and η-Te are indirect and direct semiconductors with the bandgap of 0.9 and 0.3 eV, respectively[42] (see Fig. 4(a)). Xian *et al.* theoretically predicted square selinene and square tellurene (see Fig. 4(b)) with chair-like buckled structures and nontrivial topological properties[43]. Either the massless Dirac fermions or the topological insulator phase can be realized by effective strain modulation in square tellurene[44]. Recently, experiment confirmed that this buckled square tellurene can exist stably on the CdTe interfaces[45].

Using DFT methods, Jiang *et al.* proposed a class of novel 2D tellurenyne MLs composed of atomic Te chains through noncovalent bonds[46] (see Fig. 4(c)). It was found that the electrostatic constituent of interchain binding is comparable to the vdW one, enabling the remarkable stabilities and carriers transport of tellurenyne MLs. With higher carrier mobility than black phosphorene (BP), the largest anisotropy in any existing materials and the giant Rashba spin splitting, tellurenyne has great application potential in electronics and spintronics.

Besides the tellurene MLs mentioned above, some 2D Te few-layer (FL) structures with excellent properties have been found[16, 47, 48], shown in Fig. 5. Here, it should be noted that the named rule of the FL tellurene is based on their space group and their relationship with the bulk Te[49], different from that of ML tellurene in above Zhu *et al.* and other groups. Besides, ML α-, β- and γ-Te named by Zhu *et al.* are also the ML forms of FL γ-, β- and ε-phases, respectively. The FL α-, β- and γ-phases with good environmental stabilities succeed a majority of striking properties that BP provides and could be feasibly fabricated by simple solution-based methods. Among them, the FL α-phase is a nearly direct bandgap semiconductor with extraordinary high mobility, high optical absorbance, inherent anisotropy, low-cost fabrication and tunable bandgap[16], which may urge novel properties and exciting opportunities for the research on layered materials.

These 2D FL Te can be originated from the reconstitution of crystal surfaces of trigonal Te-I. Both γ-phase and ε-phase can be obtained by cutting along the [0001] direction. β-phase and δ-phase can be formed by cutting along the [1010] and [1120] directions, respectively[47]. The β-phase with centrosymmetry prohibits a nonzero electric polarization. The ML α-phase is instable and can be transformed into ML β-phase without barrier[16]. The β-phase bilayer, however, is unstable resisting against a transition into the α-phase bilayer with broken centrosymmetry.

For 2D α- and β-phase FL tellurene, further studies have found that it can be stabilized by hole or electron doping[48]. For the bilayer, the stabilities of β-, α-, γ- and δ-phases decrease with the bandgap variations exceeding 1 eV. For the trilayer, a novel metallic chiral α+δ phase can be formed with the appearance of chirality. In the perspective of wavefunc-

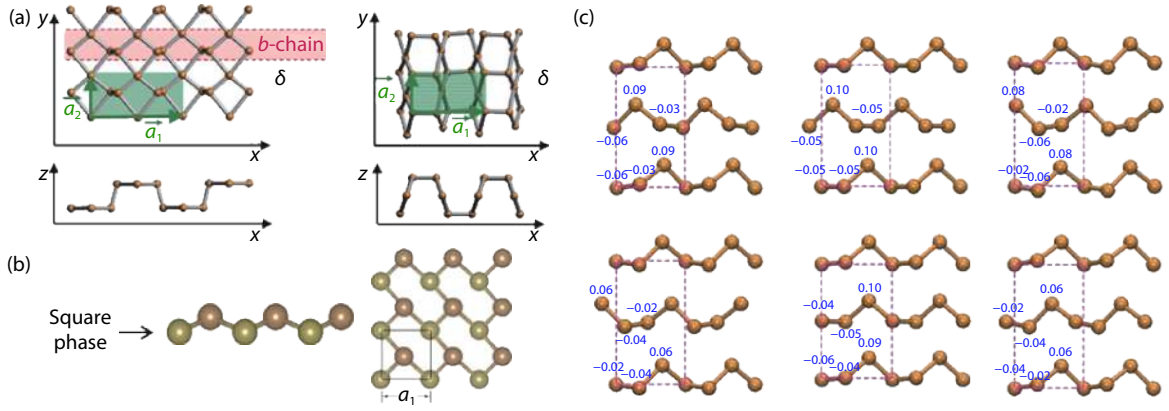

Fig. 4. (Color online) Te ML structures: (a) δ- and η-Te[42], (b) square tellurene[43], and (c) six types of tellurenyne[46].

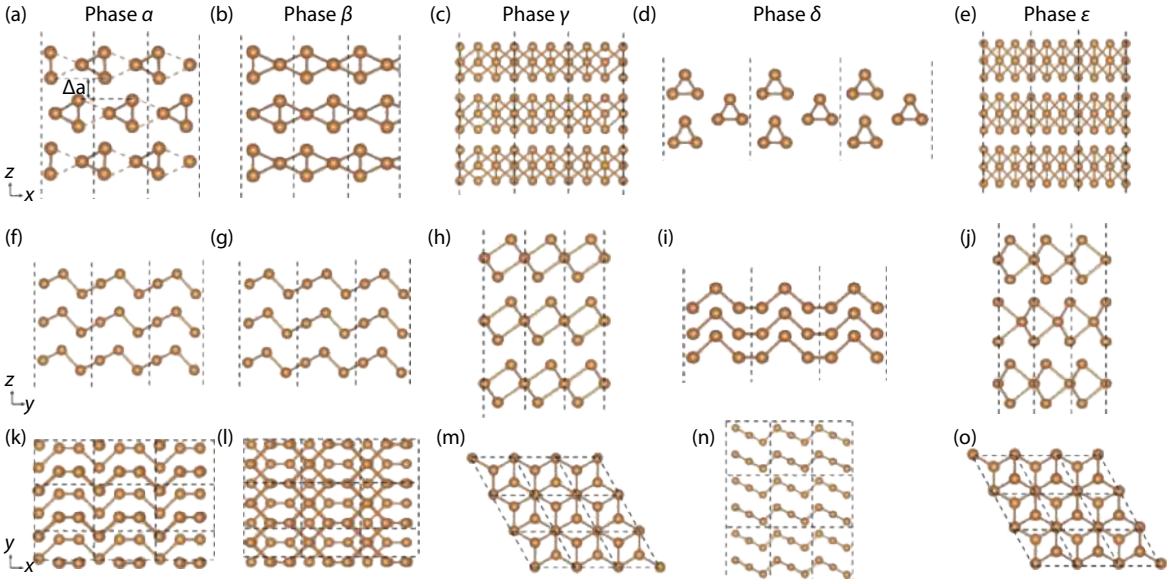

Fig. 5. (Color online) Three-layer α, β, γ, δ, and ε phases of Te[47].

tion, transitions among these phases are followed by emergence or disappearance of inversion centers (α–β, α–γ, α–α+δ), structural anisotropy (α–γ, γ–δ) and chirality (α–α+δ), which must give rise to substantial changes in the related properties.

Based on first-principles calculations, Wu *et al.* designed a highly kinetic stable layered Te bulk structure named β-Te bulk, like other layered bulk materials such as graphite. Bulk β-Te is a semiconductor with the bandgap of 0.325 eV, whose ML structure is 2D β-Te[50].

The diverse 2D structures of tellurene not only enrich the 2D material family, but also provide candidates to meet the different functions for electronics.

2.4. Experimental synthesis

The purpose of exploring 2D materials with excellent performances is their massive applications in highly integrated 2D devices. To this end, it is crucial to realize the experimental preparation of large-size 2D materials with uniform characteristics. Owing to the intrinsic structural anisotropy, 1D Te nanostructures were predominantly yielded by previously reported synthetic methods[51–53] before 2D tellurene discovered. In 2014, 2D Te hexagonal nanoplates were successfully realized on flexible mica sheets via vdW epitaxy[54], which, however, have large thickness (30–80 nm), small lateral dimensions (6–10 μm), and high roughness[55].

The top–down mechanical exfoliation method plays a pioneering role in discovering 2D MLs, which is still adopted to fabricate tellurene. Churchill *et al.* exfoliated ultra-thin Te flakes from trigonal Te single crystal, with the thicknesses ranging from 1 to 2 nm and the widths smaller than 100 nm[56]. Yang *et al.* derived 2D Te nanosheets with an average radius about 150 nm and the thickness about 10 nm[57]. Besides of mechanical exfoliation, liquid-phase exfoliation (LPE) method provides a way for massive production on 2D materials. Xie *et al.* realized the nonlayered 2D ultrathin Te nanosheets from the Te bulk by LPE, which cover the broad lateral size changing from 41.5 to 177.5 nm and the thickness ranging from 5.1 to 6.4 nm[58]. Other groups also obtained Te nanosheets by virtue of the facile and cost-effective LPE method[59, 60]. However, it is still challenge to produce high quality ML tellurene by exfoliation methods.

By a substrate-free solution process or hydrothermal method, Ye *et al.* fabricated free-standing, large-area and high-quality ML and FL tellurene, and the tellurene-based transistors can be stable for over two months at room temperature, also presenting the excellent properties including high on/off

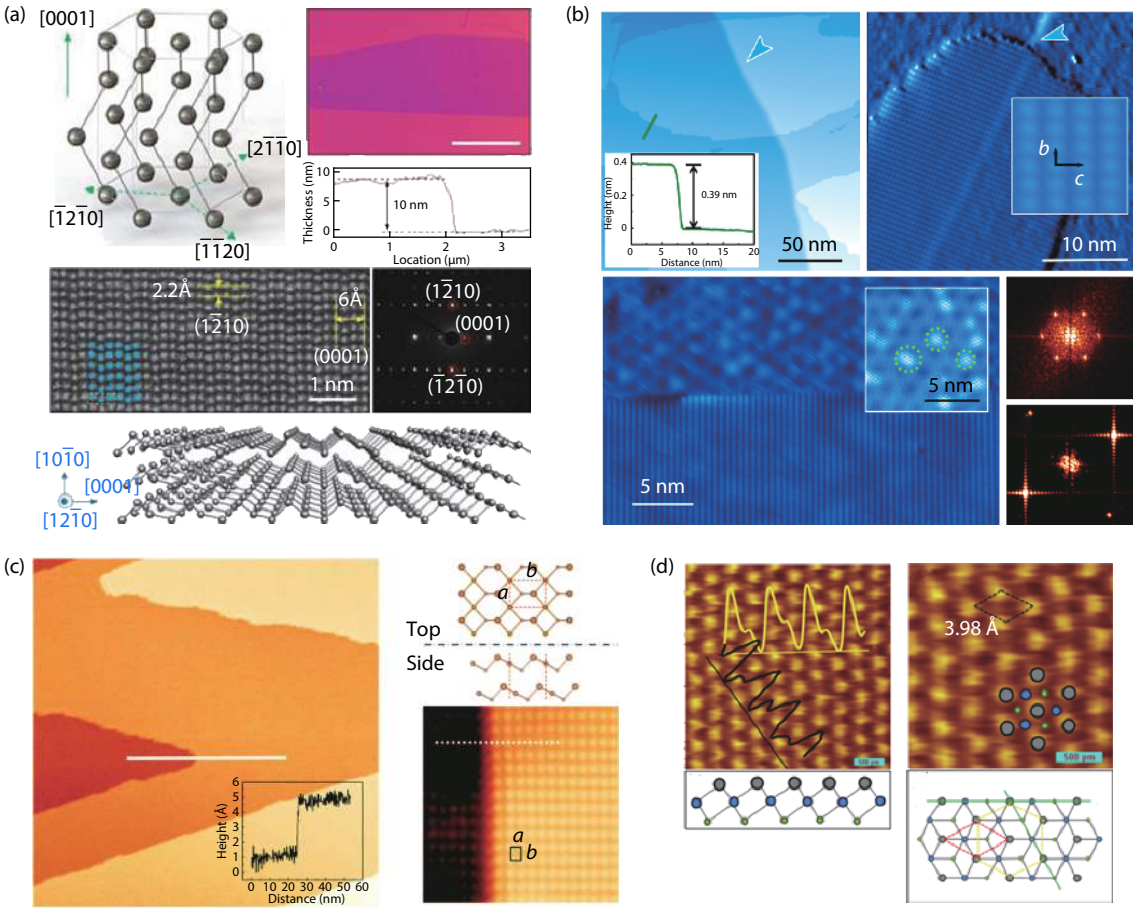

Fig. 6. (Color online) (a) Large-area 2D tellurene obtained from solution-grown method and material characterization[61], and (b) topographic images of Te films on graphene[65]. (c) Topographic image of an epitaxial Te film as well as the crystal lattice[66]. (d) Atomically resolved STM topography of a section of tellurene nanoflake and the corresponding lattice[67].

ratios, large current densities and high carrier mobilities[61] (Fig. 6(a)). Although this emergent solution-grown tellurene exhibits the above charming features, the essential manufacturing science of the hydrothermal preparation process for tellurene is still elusive. To tackle this issue, Wang *et al.* carried out firstly the systematic data-driven learning the process-structure-property relationship of solution-grown tellurene through a holistic approach integrating both the experimental explorations and data analytics, revealing the effects of process factors on production yield, dimensions and transistor-relevant properties[62]. The fundamental information is helpful to develop tellurene-based transistors with optimal and reliable property. By a hydrothermal method, Feng *et al.* synthesized the 2D Te nanosheets with the diameter of lateral dimension > 1 μm and the thickness about 40 nm[63]. By the one-pot hydrothermal reduction method, Wang *et al.* effectively synthesized 2D thin tellurene which has the hexagonal structure[64].

Vapor deposition is one of the main methods for preparing thin film materials. It has been proved that physical vapor deposition method (PVD) including molecular beam epitaxy (MBE) is also employed to produce 2D tellurene. Guo *et al.* obtained β-tellurene ML and FL thickness by MBE on the graphene/6H-SiC(0001) substrate[65] (Fig. 6(b)), and found the bandgap of tellurene films monotonically increases with the thickness decreasing, covering the near-infrared band. An explicit edge band bending between ML Te and graphene substrate has been observed. Also, Dai and Xie *et al.* applied MBE technology to grow tellurene films on HOPG substrate, whose size coincides with the β-tellurene structural parameters (Fig. 6(c))[66].

Using horizontal PVD method, Tongay *et al.* revealed that highly crystalline and self-oriented tellurene sheets can be grown on the GaS and GaSe vdW surfaces resulting from the much-reduced total energy and a stronger degree of coupling between adjacent layers[68]. A remarkable structural anisotropy can be found in the synthesized tellurene sheets. Ultrathin Te films were synthesized by Apte *et al.*, which include atomically thin Te trilayers by PVD and larger-area films by pulsed laser deposition (PLD)[69]. PVD can produce α-tellurene flakes with distinct boundaries while PLD leads to uniform and contiguous centimeter square films with the thickness of sub-7 nm. Pal *et al.* fabricated nonlayered ML α-tellurene through the anisotropic ultrasonication method (see Fig. 6(d))[67], which has so far been predicted to present a topologically insulating state with an insulating interior and metallic edge states propagating along the perimeter of the 2D objects. It should be noted that the PVD method of preparing 2D tellurene is very demanding to the growth environment and epitaxy substrates.

In addition to the above exfoliation method, solution method and vapor deposition method, some other preparation methods of tellurene have been developed. For instance, Wu *et al.* achieved ultrathin Te film with large area and clean

Table 1. Elastic stiffness constant C_{ij}, and the ideal tensile stress (ITS) and critical strain (CS) of ML α-, β-, and γ-Te[71].

	C_{11}	C_{22}	C_{12}/C_{21}	C_{66}	ITS (GPa)		CS (%)	
					Armchair	Zigzag	Armchair	Zigzag
α-Te	61.90	62.46	17.31	30.42	6.7	7.12	26	30
β-Te	32.44	72.13	18.99	17.50	7.23	11.43	36	35
γ-Te	49.42	47.43	19.32	21.39	3.25	4.49	12	24

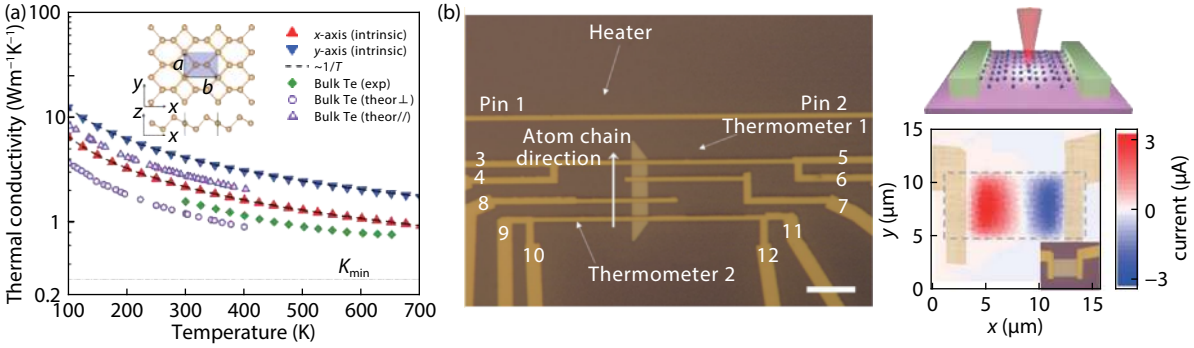

Fig. 7. (Color online) (a) Lattice thermal conductivity of tellurene versus temperature[72]. (b) Device structure and pin-out diagram, the experiment setup schematics, and the LIFE current mapping of the real device[75].

interface through a topotactic transformation, where 2D Te structure came from layered MTe_2 (M = Ti, Mo, W, etc.) matrix by the excessive lithiation[70]. The resultant ultrathin Te films with large lateral size about several tens of microns and various thicknesses ranging from ML to several tens of nanometers were achieved. Notably, the photoresponse of Te nanosheets presents negative behavior when thickness < 5 nm, while it changes to positive as thickness increases.

3. Performance and applications of tellurene

Tellurene is an outstanding 2D elemental material, which simultaneously overcomes the shortcomings such as the zero-bandgap of graphene, the instability of BP in air condition, and the small carrier mobility of MoS_2. The measures on tellurene properties have been explored.

3.1. Mechanical properties

He *et al.* studied the strain-induced mechanical property variations in ML tellurene using first-principles calculations[71]. Compared to α- and γ-Te, β-Te ML possesses the most obvious anisotropy (see Table 1), originating from its inherent structure characteristic. β-Te can endure high critical strain up to 36% and 35% along the armchair and zigzag directions, and the corresponding Young's moduli are 55 and 27 GPa, respectively. High critical strain and small Young's modulus show that β-Te ML possesses good toughness and high flexibility. Furthermore, under the strain smaller than 15%, the easily stretched direction has a reversion, which may result from the puckered structure competing with the transfer charge resistant to deformation. Interestingly, it was found that Poisson's ratio is negative in the direction out of plane when the strain is parallel to the pucker of β-Te, resulting from its hinged structure.

3.2. Thermoelectric characteristics

Due to a high value of thermoelectric figure-of-merit ZT, trigonal Te bulk is considered to be a remarkable thermoelectric material. In the light of recent progresses in the synthesis route of 2D tellurene films together with the increasing trend of utilizing nano thermoelectric devices, there is a growing interest in the thermoelectric properties of 2D tellurene.

Based on first-principles calculations and phonon Boltzmann transport, Ren and Liu *et al.* revealed the ultralow thermal properties in the ML β-Te, shown in Fig. 7(a)[72]. They predicted that it has the lowest thermal conductivity in any reported values of 2D materials, in which optical phonons play a key role, sparking off superb thermoelectric performance of tellurene[73]. Through the quasiharmonic approach, it was revealed that ML β-Te presents large positive thermal expansion at high temperature, whereas the linear and negative thermal expansion along the armchair direction at very low temperature[74]. Along the zigzag direction, the linear thermal expansion coefficient is up to 4.9×10^{-5} K^{-1} at 500 K, quite large in the full spectrum of 2D materials. The in-plane anisotropy, thermal expansion and mechanical properties of β-Te are weakened with temperature increasing, which is determined by the generalized mode Grüneisen parameters. Experimentally, in Te nanofilms, the room-temperature power factor and zT value are 31.7 μW/(cm·K^2) and of 0.63 measured for the first time, respectively (Fig. 7(b))[75]. It was also found that high work function metals can form rare accumulation-type metal-to-semiconductor contacts with Te, which enable thermoelectrically generated carriers to be collected more efficiently.

Chai *et al.* showed the three-phonon limited thermal conductivity of both square selenene and tellurene by DFT calculations[76]. The distinguished anharmonic phonon scattering process makes tellurene present the lowest lattice thermal conductivity in all the 2D elemental materials. The special square unit cell brings about a highly anisotropic electronic property between the zigzag and armchair directions. The large effective mass and Seebeck coefficient along the armchair direction mean the better thermal performance than that along the zigzag direction. These findings pave a way for tuning the thermoelectric properties of tellurene in the future.

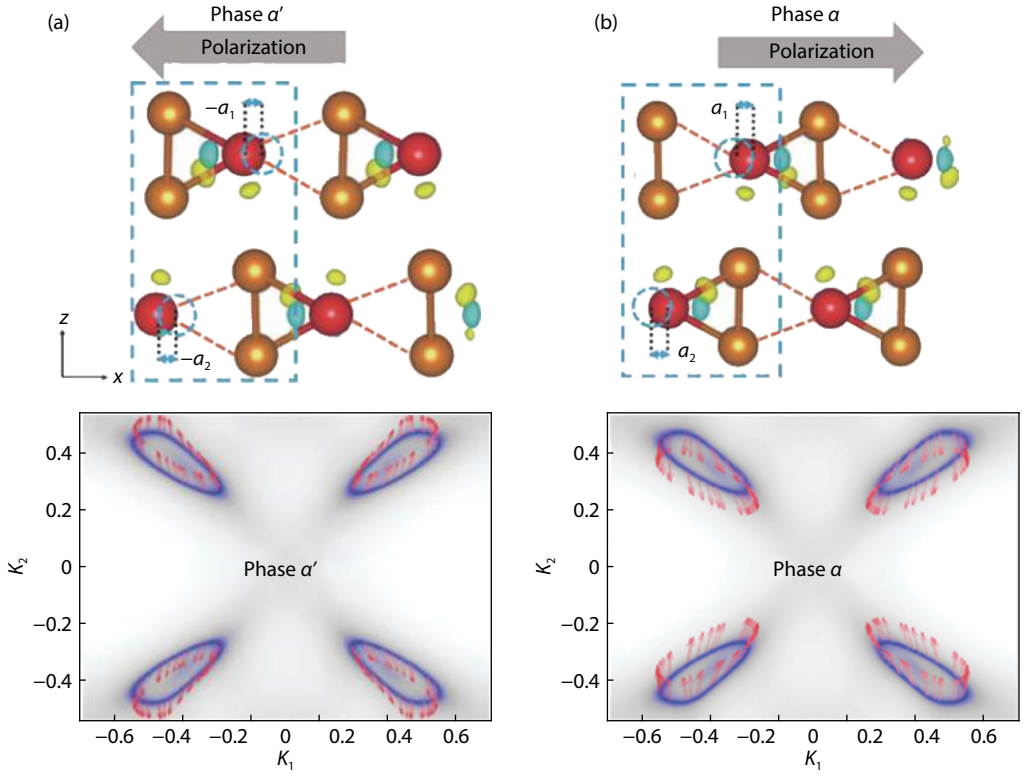

Fig. 8. (Color online) Differential charge density and spin-texture of bilayer Te phases[47].

3.3. Ferroelectric properties

Due to far-reaching implications in industrial application, ferroic materials have been one of the most important topics in condensed matter physics. The rapid development of 2D materials makes it provide unique 2D ferroelectric property due to the quantum confinement.

Although 2D Te ML structure has no ferroelectricity, the strong ferroelectricity in 2D Te FL (based on the named rule of space group) is introduced by spontaneous in-plane polarization owing to the interlayer interaction of lone pairs (see Fig. 8)[47]. The estimated polarization magnitude reaches to 2.04×10^{-10} C/m, which can be measured by the current experimental method[77]. The bilayer Te film can preserve the spontaneous ferroelectric (FE) polarization even above room temperature. Thanks to the strong SOC of Te, there exist nontrivial valley-dependent spin-textures in the hole carriers (see Fig. 8), connected with the FE polarization direction tuned by an external electric field. In the Te multilayer, both the stable FE and anti-FE phase coexists. The polarization magnitude is 1.02×10^{-10} C/(m·layer) in FE phase, while the upper and lower parts in the anti-FE phase have the opposite directions of spontaneous polarization, resulting in the zero macroscopic spontaneous polarization. At ground state, Te multilayer film is in stable FE phase. And the anti-FE phase can be induced by simple physical means such as electron doping and photoexcitation[78]. These results introduce the concept of ferroelectricity into elemental systems as well as expand the 2D FE family and provide a hopeful platform for future electronics.

Based on DFT, strain can induce the transition from β-Te ML with centrosymmetry to α-Te ML without centrosymmetry. Meanwhile, 2D ferroelectrics can form, in which the magnitude of polarization can reach up to about 90 μC/cm^2 by a tensile strain, resulting in a giant piezoelectric effect that is two orders of magnitude stronger than that of MoS_2 ML[79].

3.4. Transport properties

Normally, the electron and hole transportations along the chemical bond direction are much faster than those along the other directions in anisotropic materials. However, due to the delocalized lone pair electrons, Liu *et al.* observed that intrachain and interchain directions exhibit nearly isotropic electrical transport in trigonal Te composed of helical atomic chains, which originates from similar effective masses and potentials of charge carriers in different transporting directions[80]. The delocalization not only strengthens the interchain binding but also enables diffusion of defects across the chains, which as well as the fast intrachain diffusion facilitates these defects self-healing rapidly at low temperature.

Due to the striking characters, 2D tellurene is deemed to be a promising channel candidate of post-silicon FETs. By performing exact *ab-initio* quantum transport simulations, the performance limits of sub-5-nm ML tellurene metal–oxide–semiconductor FETs (MOSFETs) were explored. It was found that the optimized p-type ML tellurene MOSFET satisfies both the high performance and low power which the International Technology Roadmap for Semiconductors requires at a gate length of 4 nm with a negative capacity dielectric (see Figs. 9(a)–9(c))[81]. Hence, ML tellurene as the channel material offers a new route for continuing the Moore's law to 4 nm.

Quantum Hall effect (QHE) is a macroscopic manifestation of quantized states only occurring in confined 2D electron gas (2DEG) systems. At low temperature, QHE is experimentally hosted in the 2DEG with high-mobility and large external magnetic field. Due to the easy accessibility of thin films with the thickness of ML or FL at the 2D quantum limit,

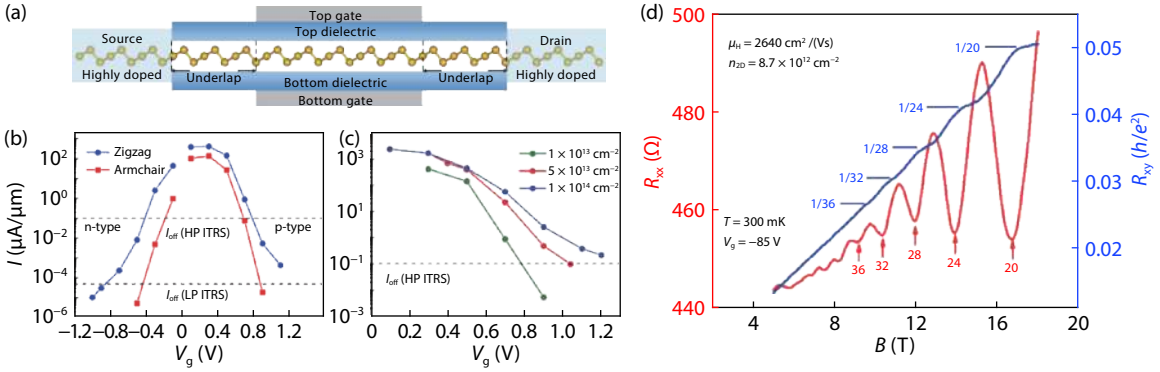

Fig. 9. (Color online) (a) Schematic view of the double-gated ML tellurene MOSFET. (b, c) Transfer characteristics of the corresponding MOSFETs with 5 nm gate length[81]. (d) QHE and SdH oscillations obtained in the 10 nm thick tellurene flake[82].

2D vdW materials are considered to be interesting material systems for studying quantum transport because they could reveal unique host material properties. Ye *et al.* for the first time directly observed QHE in the thin 2D tellurene films synthesized by hydrothermal method, which present high-quality and high hole mobility of nearly 3000 $cm^2V^{-1}s^{-1}$ at low temperatures. The interplay between the Zeeman effect and SOC causes anomalies in both temperature-dependent oscillation amplitudes and transport characteristics (see Fig. 9(d))[82].

Based on solution-grown tellurene flakes with the thickness < 30 nm, Frisbie *et al.* fabricated and characterized high-performance electrolyte-gated transistors (EGTs)[83]. It was shown that by tuning gate voltage tellurene, EGTs can cross the insulator–metal transition, achieving mobility up to ~500 $cm^2V^{-1}s^{-1}$. Particularly, a truly metallic 2D state was observed at gate-induced hole densities larger than 1×10^{13} cm^{-2}, which was verified by the temperature dependent resistance and magnetoresistance measurements. Thus in EGTs the electronic ground state of tellurene in wide-range can be tuned, offering new methods to control its physical properties electrically.

Fascinating properties can be found in atomic chains formed in a spiral shape, such as phases hosting localized bound states in their electronic structure. By the nearest-neighbor tight-binding approximation, strict conditions for a topological phase hosting zero-energy edge-bound modes were identified in a generic single atomic helix[84], and it was further shown how the 0D state restricted to the edge of a single 1D helical chain of Te atoms develops to 2D bands restricted to the *c*-axis surface of the 3D trigonal bulk[85]. By exploiting confinement to a virtual bilayer, an effective Hamiltonian description of its dispersion in *k* space was given, and the diminished SOC role was elaborated. Seminal experiments ignore the interpretation of these intrinsic gap-penetrating surface bands, where 2D transport is however ascribed to extrinsic accumulation layers.

Nakayama *et al.* carried out high-resolution angle-resolved photo emission spectroscopy on the trigonal Te composed of helical chains[31]. From the 3D band structure, they found a definitive evidence for the band splitting and the presence of Weyl nodes and small spin-polarized hole pockets near the H point. The finding opens a pathway to study the interplay among the crystal exotic physical properties in chiral materials.

Dirac and Weyl nodal materials can host low-energy relativistic quasiparticles. The topological properties of Dirac/Weyl materials can directly manifest through quantum Hall states under strong magnetic fields. However, most Dirac/Weyl nodes generically exist in semimetals without exploitable bandgaps due to their accidental band-crossing origin. Tellurene possesses chiral crystal structure which induces unconventional Weyl nodes with a hedgehog-like radial spin texture near the conduction band edge. Ye *et al.* experimentally observed Weyl fermions in the synthesize high-quality n-type tellurene by a hydrothermal method with subsequent dielectric doping, and detected a topologically non-trivial π Berry phase in quantum Hall sequences[86]. This work expands the spectrum of Weyl matter into semiconductors and offers a new platform to design novel quantum devices by marrying the advantages of topological materials to versatile semiconductors.

Due to Te intrinsic p-type nature, few people experimentally studied its conduction band (CB). By atomic layer deposited dielectric doping technique, the CB transport properties of 2D Te can be accessed in a controlled fashion. In n-type 2D Te films, Ye *et al.* performed a systematic study on the weak-antilocalization (WAL) effect[87], and found that the WAL is in line with Iordanskii, Lyanda-Geller, and Pikus theories, depending on the gate and temperature which reveals that D'yakonov-Perel mechanism is predominant in spin relaxation and electron-electron interaction determines phase relaxation. At $T = 1$ K, they achieved large phase coherence length near 600 nm, as well as gate tunable spin-orbit interaction (SOI) and observed weak-localization (WL) transforming into WAL. These findings manifest a new controllable strong SOI 2D semiconductor with high potential for spintronic applications, which is provided by newly developed solution-based synthesized Te films.

Using many-body perturbation theory based on first-principles, Lu *et al.* investigated the evolvement of the relationship between quasipartile energies and excitons evolving as the dimensionality of Te nanostructures changes[88]. It was revealed that even though the atomistic structures are similar, both many-electron interactions and excited-state properties are enhanced with dimensionality decreasing. The self-energy correction of the bandgap is 0.22 eV in bulk, reaching to 0.90 eV in 2D ML and finally to 2.70 eV in 1D spiral tube. The exciton binding energy less than 10 meV in bulk means the weak excitonic effects, which however is significantly increased to 0.67 and 2.40 eV in the ML and 1D structures, re-

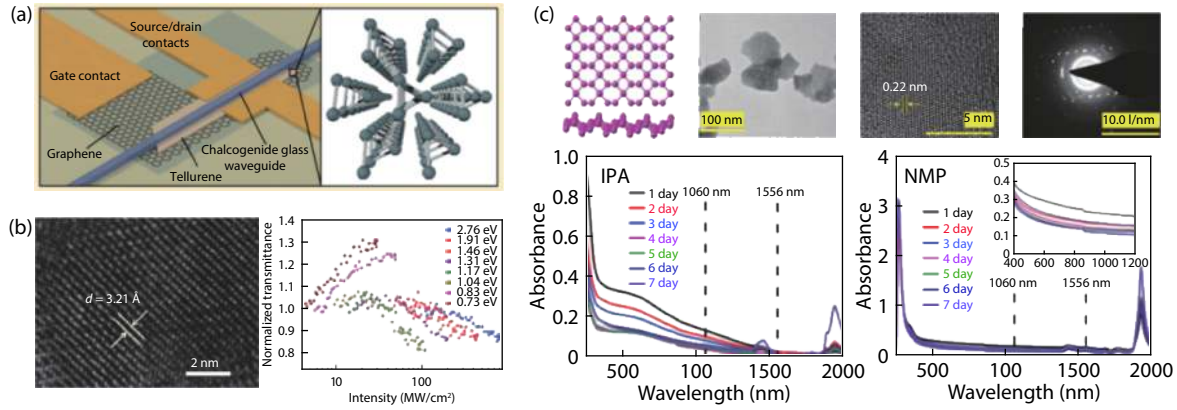

Fig. 10. (Color online) (a) Diagram of waveguide integrated tellurene photodetector, in which the inset is top view of crystal structure of tellurene along [0001] axis[89]. (b) HR-TEM image for tellurene nanosheet, and the normalized transmittance as a function of excitation energy density of tellurene nanosheets with different photon energies[59]. (c) Characterization of 2D Te nanosheets together with 2D Te/PVP membrane[60].

spectively. Importantly, dimensionality reduction also produces significantly anisotropic optical response through many-electron interactions.

3.5. Optical properties

2D tellurene is a promising and versatile material, which offers a platform for mid-infrared photonics. The waveguide-integrated tellurene photodetector and Pockels effect modulator were designed (See Fig. 10(a))[89]. At 3 μm wavelength, the noise equivalent power of the photodetector is 0.03 fW/Hz$^{1/2}$ at room temperature. Meanwhile, a half-wave voltage-length product ($V_\pi L$) and a switching energy are 2.7 V·cm and 12.0 pJ/bit in the optimized modulator device, respectively, which both mean significant enhancements for current state-of-the-art devices.

Nonlinear optics is widely used in laser, information and material technologies. 2D nanomaterials have excellent wideband nonlinear saturation absorption properties, which can be made into the saturable absorber (SA) of Q-switched and mode-locked fiber lasers producing different wavelength pulses, such as graphene[90], TMDs (MoS_2 and WS_2)[91], topological insulators (Bi_2Se_3)[92] and phosphorene[93]. Recently, it has been found that tellurene presents the nonlinear optical properties.

Firstly, as a result of the strong interaction between light and matter from visible to infrared range, the unique 2D Te-based nonlinear photonic device with room temperature stability can act as photonic diode and all-optical switcher[94]. This photonic diode can be applied in the non-reciprocal optical propagation of telecommunications or integrated photonics. Furthermore, for all-optical switching operation, one can successfully realize "ON" and "OFF" modes in 2D Te-based light-modulate-light device. Secondly, by virtue of open-aperture Z-scan technology, the nonlinear absorption features were explored in fabricated 2D ultrathin Te nanosheets[59] through liquid-phase exfoliation method as well as Te/polyvinylpyrrolidone (Te/PVP) membrane[60] (See Figs. 10(b) and 10(c)). Excellent broadband saturated absorption and optical limiting behaviors can also be found in Te nanosheets, in which the superiority of the infrared range as a SA is highlighted by the low saturable intensity and large modulation depth of saturated absorption with low energy photon excitation. Additionally, owing to a clear two-photon absorption behavior in the visible range with large energy excitation, tellurene can be used for an optical limit material, protecting the sensitive optical devices and human eyes. Further, it was found that this SA with high-quality can be utilized to generate ultra-short and ultra-high peak power laser pulses in fiber or all-solid-state lasers. In the 2D Te/PVP membrane, the nonlinear absorption coefficient large up to 10^{-1} cm·G/W in the spectral range of 800 to 1550 nm demonstrates the efficient broadband saturable absorptivity. Exploiting the 2D Te/PVP ultrathin film in a SA, one can obtain a femtosecond laser with high stability, which can generate the pulse duration of 829 fs in the communication band. Experimentally, the excellent tellurene-based SA can achieve Q-switched and mode-locked operations within erbium-doped fiber (EDF) lasers[95]. A modulation depth of 0.97% can be obtained in high-quality tellurene-based SA, which is inserted into the EDF laser cavity by sandwiching the Te/PVA film between two fiber ferrule, and then one can acquire either the passively Q-switched or mode-locked operations. In the passively Q-switched operation, the repetition rate is raised from 15.92 to 47.61 kHz, whereas the pulse duration is reduced from 8.915 to 5.196 μs. Furthermore, mode-locked operations are also achieved through adjusting the polarization state.

Solution-synthesized Te nanoflakes can be used as short-wave infrared photodetectors[96]. Abbas *et al.* reported that the solution-synthesized tellurene nanoflakes can be also applied in broadband and ultrasensitive photodetection[97]. At ambient conditions, the tellurene nanoflake exhibits the high hole mobility up to 458 cm^{2}V^{-1}s^{-1}, which based photodetector has the peak extrinsic responsivity of 383 A/W, 19.2 mA/W, and 18.9 mA/W at the light wavelength of 520 nm, 1.55 μm, and 3.39 μm, respectively. Profiting from the photogating effect, the high gains of 1.9×10^3 and 3.15×10^4 are derived at the wavelengths of 520 nm and 3.39 μm, respectively. At the communication wavelength of 1.55 μm, an exceptionally high anisotropic behavior and a large bandwidth of 37 MHz can be obtained in the tellurene based photodetector. The photodetection performance dependent on wavelength was also proved by the corresponding quantum molecular dynamics simulations. These results exhibit the air-stable tellurene based photodetectors completely covering the short-wave infrared range with ultrafast photoresponse.

Through DFT combined with the nonequilibrium Green's function calculation, Gao *et al.* found that tellurene bilayer

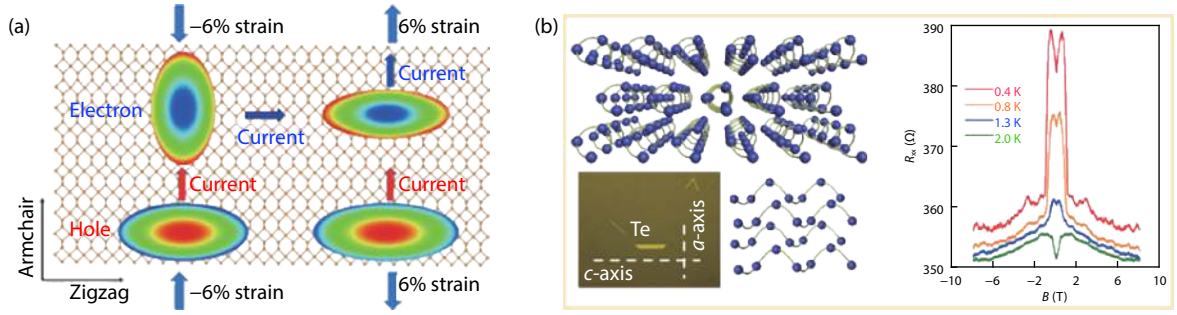

Fig. 11. (Color online) (a) Electrical conductance of β-Te ML under the compressive and tensile strains of -6% and 6%, respectively[101]. (b) Lattice structure of trigonal bulk Te as well as the optical image of Te thin film with the thickness of 22.1 nm and two principle lattice orientations on the left. Here, scale bar is 50 μm. The panel on the right is magneto-resistance of Te thin film as a function of magnetic field B_x at different temperatures[102].

presents a broad photoelectric response over the range from visible to near-infrared region[98]. Moreover, bilayer tellurene-based photodetector shows an ultra-strong anisotropic photo-responsivity and an ultra-high extinction ratio (~2812 at the photon energy of 3.4 eV), much higher than antimonene (~145) and phosphorene/blue phosphorene bilayer (~240). The ultra-strong anisotropy is attributed to the transition of Te 5p bonding orbitals, which are parallel or perpendicular to the chain direction.

By studying ambipolar tellurene based FETs, Berweger demonstrated the general ability of near-field scanning microwave microscopy to image and study the local carrier type and relevant conductivity by *operando*[99]. It was revealed that the global minimum of device conductivity relying on transport measurements results from the continued coexistence of p-type regions at the device edge and n-type regions in the interior of their micrometer-scale devices.

4. Performance modulations of tellurene

4.1. Strain effects

Strain-engineering on 2D semiconductors could further tailor their electronic properties. The strain effect on 2D tellurene with the helical chain as basic unit can induce phase transition and some exotic natures.

Based on DFT, it was manifested that the strain-induced phase transition from a centrosymmetric β-phase to a non-centrosymmetric α-phase in ML tellurene (named based on space group, and next paragraph is the same)[79, 100], which is attributed to the tensile strain induced bonding strength decreasing and the atom migration corresponding to the phonon vibration mode in the distorted direction. This strain-induced transition is also supported by the calculated electronic band structure with SOC leading to a large Rashba splitting due to symmetry breaking, which may enable the spin to be tuned via the electric field[52]. ML tellurene has strong absorption in the visible and ultraviolet regions[100], which can be significantly impacted by strain. With the strain increasing, the real and imaginary parts of the dielectric function exhibit redshift. Additionally, the compressive strain rather than the tensile strain is more likely to excite the absorption spectrum in α- and β-Te, whereas just slight differences are produced in γ-Te.

Leng *et al.* showed that in-plane compression facilitates the $\alpha \rightarrow \beta$ phase transition, whereas in-plane tensile strains invariably enable α-phase to be more stable than β-phase[49]. Nevertheless, the energy difference between the two phases amounts to or is even much smaller than the thermal energy kT. A possible transition from α to γ phase may be realized by further increasing the tensile strain in the chain direction larger than a critical value about 12%. The tensile strain above 15% will make γ-phase more stable than α-phase, along with a transition energy barrier further decreasing.

Yang *et al.* demonstrated by first-principles DFT that strain-engineering can controll the highly anisotropic electron mobility and electrical conductance of β-Te[101] (Fig. 11(a)). At the strain between −1% and 0%, the direction of electrical conductance of β-Te can be transformed armchair into zigzag direction. And the bandgap of β-Te undergoes an indirect-direct transition, which enables the effective masses tensor to rotate. Meanwhile, an important role of the deformation potential constant is also played in the electrical conductance anisotropy rotating. Under strain, the anisotropic hole conductance is impregnable. These findings indicate that β-Te with the high anisotropic carrier mobility and superior mechanical flexibility is a promising candidate for flexible nanoelectronics.

Through experimental demonstrations of 1D vdW Te by Raman spectroscopy under strain and magneto-transport, pronounced strain response along the *c*-axis and no strain response along the *a*-axis were observed due to the strong intra-chain covalent bonds and the weak interchain vdW interaction, respectively. And magneto-transport results also confirmed its anisotropic property, resulting in obviously different magneto-resistance behaviors in three different magnetic field directions. Specifically, phase coherence length of $L_\phi \approx T^{-0.5}$ was obtained from weak antilocalization effect, indicating its 2D transport characteristics under an applied magnetic field normal to the thin film. By comparison, $L_\phi \approx T^{-0.33}$ from universal conductance fluctuations was obtained under the magnetic field in the *c*-axis, which indicated its 1D transport nature along the helical chain. From experimental perspectives, the 1D vdW structure is strongly evidenced by these studies obtained from the single crystal Te thin film with high quality[102] (see Fig. 11(b)).

4.2. Defect effect

Due to the atomic level dimension, the effects of vacancies and common adsorbates in ambient conditions and functional group play a significant role in 2D material based devices.

A comprehensive study on the adsorption of nineteen typ-

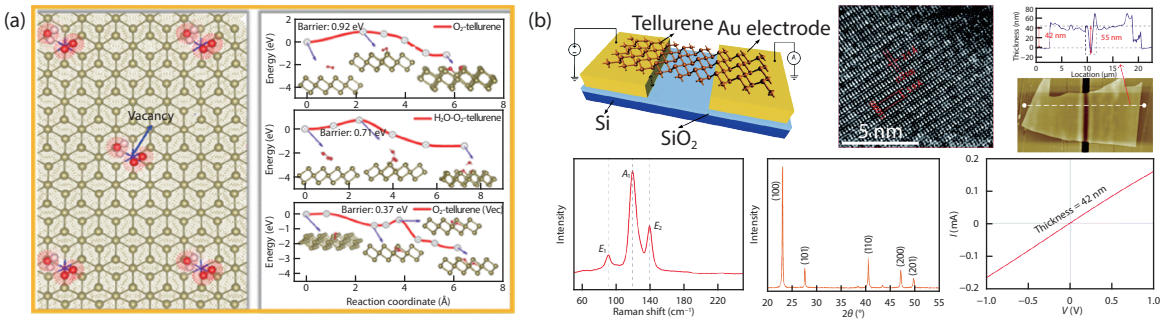

Fig. 12. (Color online) (a) Adsorption configurations of H_2O and energy barriers for dissociation of O_2 on the tellurene surface[104]. (b) Schematic and morphological characterization of tellurene based sensors[105].

ical adatoms and five typical molecules of H_2, O_2, H_2O, NO_2, and NH_3 adsorbed above ML α-Te and β-Te using first-principles based on DFT could be found in Ref. [103]. It was revealed that diverse electronic states can be induced by these adatoms, such as n-type doping, p-type doping, half-metal, and spin-gapless semiconductor features. The molecules of H_2O and O_2 behave essentially different on tellurene, and water adsorption can be evidently enhanced by adjacent pre-adsorbed O_2, shown in Fig. 12(a)[104]. The Te vacancies forming can enhance the adsorption of both O_2 and H_2O molecules. Furthermore, the coexistence of H_2O and Te vacancies can greatly enable the dissociation of O_2, indicating that tellurene may be easily oxidized under humid conditions. Additionally, vacancies can induce significant modification on the electronic propertes of tellurene, which, however, are well maintained upon either H_2O or O_2 adsorption on its surface.

Performing DFT and molecular dynamics simulations, Ataca *et al.* investigated the stabilities and electronic properties of α- and β-tellurene ML as well as the corresponding H, O, and F functionalized counterparts, including SOC effects[106]. Their results showed that perfect semiconducting α- and β-Te MLs can be tuned into metallic properties due to functionalized counterparts, except for the hydrogenated β-Te semiconductor with a bandgap of 1.37 eV. H, O and F functionalization can destabilize the structure of α-Te, the introduction of F and H can make β-Te layers evolve into functionalized atomic chains, and O can oxidize β-Te leading to a Te_3O_2-like structure. Tellurene MLs as well as their functionalized counterparts have potential applications in both future optoelectronic devices and metallic contacts of nanoscale junctions.

Chemiresistive sensor devices made from 2D materials have been extensively investigated. Neverthless, no single material has all the desirable attributes until the discovery of tellurene. The puckered structure of tellurene offers Te atoms different coordination environments on the surface, which would be propitious to sense. Wang *et al.* found that tellurene succeeds in a sensor for detecting NO_2 (See Fig. 12(b))[105]. Tellurene based devices show a detection limit of 25 ppb, a great detection scope from 25 ppb to 5 ppm, a baseline noise as low as 0.5%, and an outstanding selectivity to NO_2 even the existence of cross-contaminants. DFT calculations manifest that large adsorption energy and intense charge redistribution can explain why the sensitivity and selectivity of tellurene for NO_2 detection are so high. Further, heat-pulsing enables fast sensor response and recovery time while does not damage the tellurene sheets. Above all, the tellurene with extraordinary air-stability is a promising candidate for next-generation chemical sensors.

Due to the high chemical stability and excellent electrical characteristics, SF_6 has been widely used in gas insulated switchgear. Whereas the electric arc and corona can normally decompose SF_6, generating HF, SOF_2, SO_2, SO_2F_2, H_2S, etc., which could corrode the medium in the ninternal equipment[107]. The results based on DFT calculations revealed that ML tellurene is preferable for the SF_6 decomposition components above mentioned. And especially for SO_2 and SOF_2, tellurene exhibits favorable adsorption strength and distinct charge transfers[108]. Meanwhile, the electronic properties of tellurene are obviously changed after SO_2 and SOF_2 adsorption.

4.3. Te nanostructures

Like other nanoribbons obtained from 2D material, the stabilities of both ML and bilayer tellurene nanoribbons (TNRs) mainly depend on their widths[109] (see Fig. 13(a)). In disregard of width, tip TNRs behave as metals, whereas notch TNRs behave as p-type conductors. Amusingly, both ML and bilayer chain TNRs are semiconductors, which can transform into metals with the width increasing. For tip and notch TNRs, the electronic structures largely depend on the atomic reconstruction of the edges as well as the corresponding unsaturated electronic states. The mechanism of the semiconductor-to-metal transition in chain TNRs can be ascribed to the spontaneous in-plane electronic polarization across the ribbon. These findings demonstrate diverse electronic properties in 1D elemental Te nanostructures.

Owing to the bonding free surface carrier transport, 2D materials possess application prospect in semiconductor logic devices. However, the edge issues induced by scaling transistor width have notably restricted their surface transport in the lateral direction, causing the increase of effective mass and the bandgap fluctuating. Consequently, it is of importance to find a novel 2D material with both excellent surface transport and free of edge effect. In view of the distinctive Te–Te bonds in tellurene, the edge effect on the transport properties was theoretically studied via TNRs with four types of edge[110] (see Fig. 13(b)). Among them, three types exhibit semiconducting feature. Compared with those of graphene nanoribbons, and Si and Ge nanowires, the surface transport is almost unaffected by the tetragonal edges (TEs) in zigzag TNRs (ZTNRs), sparking off minimized bandgap and variations of effective mass. Further, by virtue of a model of metal–oxide–semiconductor transistor combined with a multis-

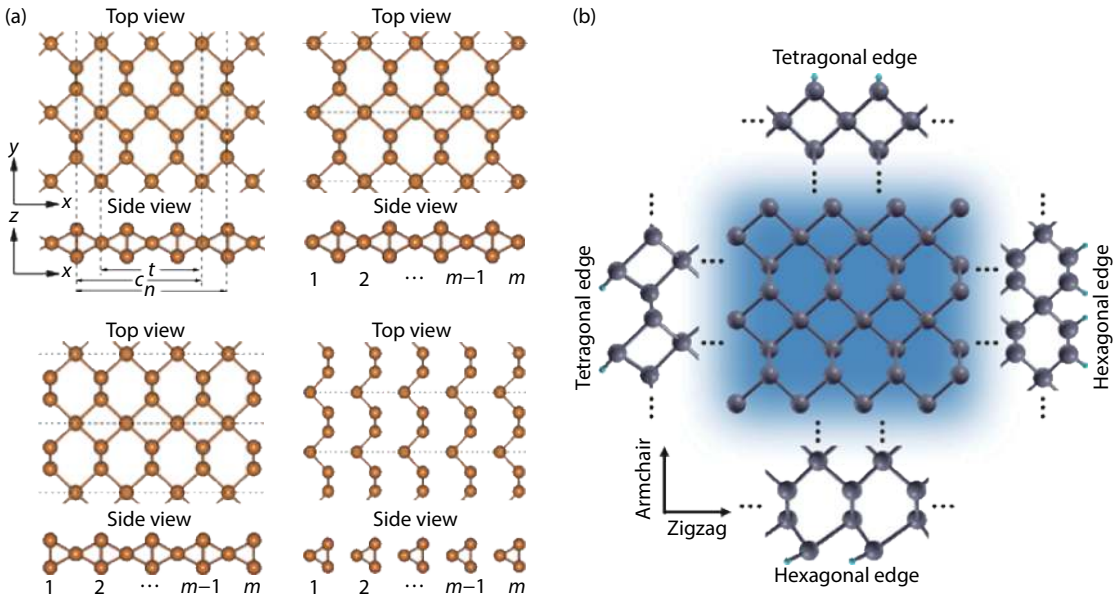

Fig. 13. (Color online) (a) Top and side views of the crystal structures for ML tellurene, and tip, notch, and chain nanoribbons, respectively. The letter *t*, *c* and *n* in ML indicate the tip, chain and notch ribbons, respectively[109]. (b) Schematic diagrams of the four edge types in TNRs[110].

cale simulation flow in the TE-ZTNRs, excellent transport behaviors were found from the calculated current densities larger than 1 mA/μm and the on–off ratios over 10^{11}. These findings indicate that the TE-ZTNRs have application perspective in nanoscale transistors.

The anomalous phase transition induced by pressure was observed in the single crystalline TNRs with high quality obtained from hydrothermal method[111]. There exist a large pressure hysteresis and multiple competing phases during the phase transition: the phase transition suddenly occurs from trigonal to orthorhombic phase at 6.5 GPa during compression, which still remains stable up to 15 GPa. Whereas phase transition gradually completes during decompression, and under the pressure from 6.9 to 3.4 GPa, orthorhombic and trigonal phases can coexist, which is also confirmed by Grüneisen parameter calculations, suggesting the hysteretic behavior of phase transition. Finally, orthorhombic to trigonal phase transition occurs at 3.4 GPa, meaning the overall pressure hysteresis of around 3.1 GPa.

Electrically manipulating charge carriers supports the operations of state-of-the-art devices. However, for charge carriers, effectively controlling interfacial energetics by the dynamic mechanical stimuli has been rarely unexplored for semiconductor nanodevices, which can be addressed by exciting opportunities offered by piezotronic effect in nanostructured piezoelectric semiconductors. Gao *et al.* for the first time explored piezotronic effect in p-type Te nanobelt experimentally and systematically investigated the strain-gated charge carriers transport properties[112]. Through the interfacial effect on the Schottky contacts and the volumetric effect on the conducting channel, the electronic transport can be modulated by the strain-induced polarization charges in the [10$\bar{1}$0] surfaces of Te nanobelt. These results allow the access to a broad range of characterization and application of Te nanomaterials for piezotronics.

4.4. Te-based heterostructures

Heterostructures by stacking two or more 2D ML materials together in transverse or longitudinal manner can provide new potentiality beyond its single ML materials[113–117]. Due to the unique structure and the large lattice constant, it is difficult to form in-plane Te-based heterostructures. Thus Te-based heterostructures mainly focus on the vertically stacking vdW heterostructures (vdWH).

In virtue of its desirable optoelectronic properties, high stability and strong visible light absorption, tellurene is considered as a promising candidate for the design of highly efficient heterojunction solar cells. Using first-principles calculations, it was found that Te/TMD vdWH presents an ideal bandgap of 1.47 eV as well as other excellent optoelectronic properties, such as the strong visible light absorption up to 5.0×10^5 cm^{-1} and the high carrier mobility up to 2.87×10^3 cm^{2}V^{-1}s^{-1} (Fig. 14(a))[118]. Most importantly, the desirable type II band alignment can be found in Te/TMD vdWHs, which results in strong charge separation and enhanced sunlight absorption. Particularly, the proposed Te/WTe_2 and Te/$MoTe_2$ vdWH solar cells show the maximum power conversion efficiencies up to 22.5% and 20.1%, respectively.

The graphene (G)/α-Te and G/β-Te interface are formed by an n-type Schottky contact with a negligible Schottky barrier height (SBH) and a p-type Schottky contact with a SBH of 0.51 eV, respectively[120]. The variation of interlayer spacing or external electric fields perpendicular to the interfaces can effectively tune both Schottky barriers and contact types at the G/Te interfaces, which is ascribed to charge transfer changing, together with the corresponding interface dipole and potential step with the external electric field and interlayer coupling. By the aid of both *ab-initio* electronic structure calculations and quantum transport simulations, Yan *et al.* for the first time thoroughly explored the interfacial characteristics between ML tellurene FETs and a series of common bulk metals along with 2D graphene as electrodes[121]. The lateral p-type Schottky contact is formed by contacting with Au in the *armchair* direction, and Cu, Ni, Ag, Pt, and Pd in both directions due to strong Fermi level pinning, whereas the lateral n-type Schottky contact is formed with Au in the *zigzag* direction and Sc in both directions. Notably, in both directions of

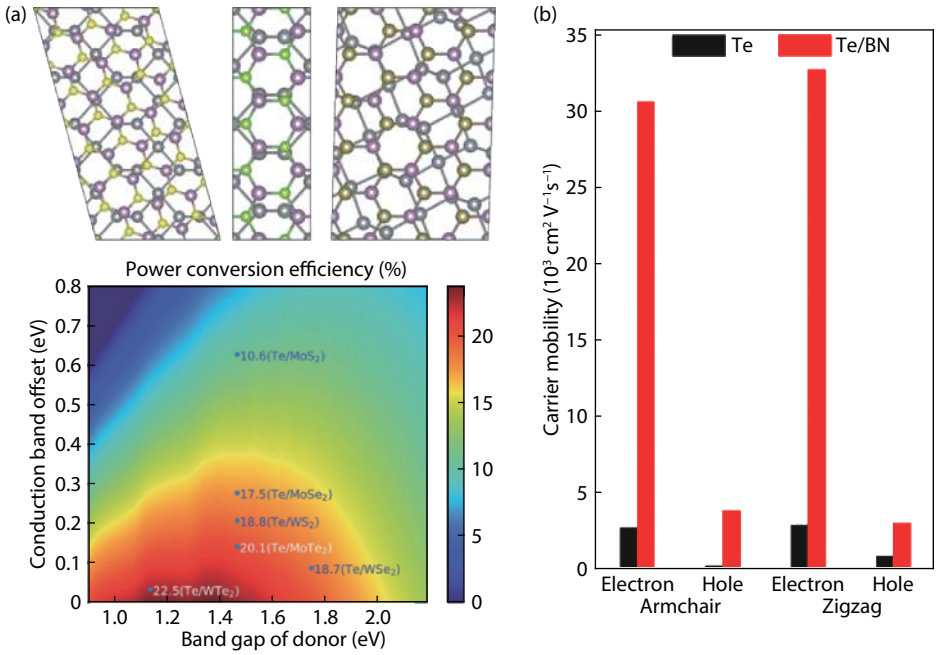

Fig. 14. (Color online) (a) Geometric structures of Te/XS_2, Te/XSe_2 and Te/XTe_2 (X = Mo or W) vdWHs (top views), and diagram of power conversion efficiency of solar cells made from Te/TMDs vdWH[118]. (b) Comparation between the carrier mobilities of the 2D α-tellurene and Te/BN vdWH[119].

tellurene contacting with graphene, a highly desirable lateral p-type Ohmic contact was found. When bilayer tellurene contacting with metal (Ag, Al, Au, and Cu), the vertical Schottky barriers occur in Ag, Al, Au, and Cu electrodes in term of the maintenance of the band structure from the noncontact tellurene layer, while a p-type vertical Schottky contact was revealed as a result of the vdW interaction for graphene electrode[122]. These investigations give comprehensions of the interfacial characteristics and guidances on electrode selection for 2D tellurene devices.

Using first-principles, the electronic and optical properties were investigated for the α-Te-based vertical vdWHs constructed by α-Te and some other 2D MLs including MoS_2[123], C_2N[124], PbI_2[125], h-BN[119], and VS_2[126]. Among them, α-Te/MoS_2, PbI_2/α-Te and α-Te/h-BN vdWHs all possess obvious type-I band alignments with the indirect bandgaps of 0.77, 0.64, and 0.59 eV, respectively, in which VBM and CBM are both from α-Te ML. Whereas α-Te/C_2N vdWH has a unique type-II band alignment, whose indirect band gap value is 1.01 eV. By the external electric field or changing the interlayer spacing, the electronic properties of these vdWHs can be tuned, including bandgap and type. Through increasing the interlayer spacing and applying an external electric field, α-Te/MoS_2 vdWH undergoes the transitions from intriguing type-I to type-II and indirect to nearly direct vdWH, respectively[123]. Surprisingly, the carrier mobilities in the Te/h-BN bilayer can reach up to 10^4 $cm^2V^{-1}s^{-1}$, one order of magnitude higher than those in tellurene (See Fig. 14(b))[119], which is induced by the dramatically increased in-plane stiffness along with the reduced deformation potential in contrast with tellurene ML. For the α-Te/C_2N vdWH, the bandgap can be modulated from 0.49 to 1.16 eV by external electric field. And under an external electric field of 0.4 V/Å, there exists a type-II to type-I transition. Interestingly, the α-Te/C_2N vdWH presents high optical absorption up to 10^5 cm^{-1} and wide band width from ultraviolet to near-infrared region[124]. Recently, VS_2 ML has attracted much attention due to its inherent ferromagnetic property[127, 128]. In the α-Te/VS_2 heterobilayer, a ferromagnetic half-metal vdWH with the type-III band alignment was revealed with a curie temperature of 150 K[126].

5. Summary and perspective

We have reviewed the theoretical and experimental works related to 2D tellurene since it was proposed by our theoretical simulations. Unlike other 2D materials with the corresponding 3D layered bulk phases, 2D tellurene has been invented in a building-a-lego-like manner. We have revealed all possible phases, different combination multilayer stackings, nanoengineering, defects and heterostructures, etc. Each will lead to its own interesting properties, which provide more options for electronic applications. Their mechanical, thermal, electronic and tranport properties have been reviewed along with the experimental realization of electronic applications combined with theoretical predictions. It outstands other 2D materials, which makes it a promising candidate for next-generation nanodevices.

It is of great importance to theoretically design more 2D structures of Tellurene as well as explore their formation mechanism, excellent properties and applications, especially the unique properties such as transport, magnetism and superconductivity. Secondly, it is still necessary to study the functionalization of the tellurene phases which have been successfully prepared by experiments, through defects, strains, heterostructures and nanoribbons, etc. The performance of the device is dependent on not only the materials but also the fabrication procedures, such as nanosheet transfer, substrates and contacts metals. Hence, the standardization of fabrication procedures is also critical, which is the common problem for all the 2D material-based devices. For the synthesis of 2D tellurene,

it is still on the way to high quality, large dimension, and massive production monolayer, which will be the bottleneck for its further massive device production.

2D tellurene provides an excellent example how theoretical calculations play the leading role in the materials discovery followed by experimental realization, even for the conventional main group element. And the research on big-data driven process-structure-property relationship will further inspire the collective efforts for open questions and improvements in the 2D tellurene as well as 2D material science in general.

Acknowledgements

This work was supported partly by the National Natural Science Foundation of China (Grant Nos. 11804082 and 11774078), by the Foundation of Henan Educational Committee (Grant No. 18A140018), and by the Doctoral Foundation of Henan Polytechnic University (B2018-37).

References

[1] Novoselov K S. Electric field effect in atomically thin carbon films. Science, 2004, 306, 666
[2] Feng B J, Zhang J, Zhong Q, et al. Experimental realization of two-dimensional boron sheets. Nat Chem, 2016, 8, 563
[3] Kamal C, Chakrabarti A, Ezawa M. Aluminene as highly hole-doped graphene. New J Phys, 2015, 17, 083014
[4] Tao M L, Tu Y B, Sun K, et al. Gallenene epitaxially grown on Si(111). 2D Mater, 2018, 5, 035009
[5] Singh D, Gupta S K, Lukačević I, et al. Indiene 2D monolayer: A new nanoelectronic material. RSC Adv, 2016, 6, 8006
[6] Vogt P, de Padova P, Quaresima C, et al. Silicene: compelling experimental evidence for graphenelike two-dimensional silicon. Phys Rev Lett, 2012, 108, 155501
[7] Bianco E, Butler S, Jiang S S, et al. Stability and exfoliation of germanane: A germanium graphane analogue. ACS Nano, 2013, 7, 4414
[8] Zhu F F, Chen W J, Xu Y, et al. Epitaxial growth of two-dimensional stanene. Nat Mater, 2015, 14, 1020
[9] Yuhara J, He B J, Matsunami N, et al. Graphene's latest cousin: Plumbene epitaxial growth on a "nano WaterCube". Adv Mater, 2019, 31, 1901017
[10] Li L K, Yu Y J, Ye G J, et al. Black phosphorus field-effect transistors. Nat Nanotechnol, 2014, 9, 372
[11] Zhang S L, Yan Z, Li Y F, et al. Atomically thin arsenene and antimonene: Semimetal-semiconductor and indirect-direct band-gap transitions. Angew Chem Int Ed, 2015, 54, 3112
[12] Ji J P, Song X F, Liu J Z, et al. Two-dimensional antimonene single crystals grown by van der Waals epitaxy. Nat Commun, 2016, 7, 13352
[13] Reis F, Li G, Dudy L, et al. Bismuthene on a SiC substrate: A candidate for a high-temperature quantum spin Hall material. Science, 2017, 357, 287
[14] Zhu Z L, Cai X L, Yi S, et al. Multivalency-driven formation of Te-based monolayer materials: A combined first-principles and experimental study. Phys Rev Lett, 2017, 119, 106101
[15] Glavin N R, Rao R, Varshney V, et al. Emerging applications of elemental 2D materials. Adv Mater, 2020, 32, 1904302
[16] Qiao J S, Pan Y H, Yang F, et al. Few-layer tellurium: One-dimensional-like layered elementary semiconductor with striking physical properties. Sci Bull, 2018, 63, 159
[17] Deng S Q, Koehler J, Simon A. Unusual lone pairs in tellurium and their relevance for superconductivity. Angew Chem Int Ed, 2006, 45, 599
[18] Coker A, Lee T, Das T P. Investigation of the electronic properties of tellurium: Energy-band structure. Phys Rev B, 1980, 22, 2968
[19] Hulin M. Electron band structure of tellurium. J Phys Chem Solids, 1966, 27, 441
[20] Beissner R E. Electron energy bands in tellurium. Phys Rev, 1966, 145, 479
[21] Junginger H G. Electronic band structure of tellurium. Solid State Commun, 1967, 5, 509
[22] Weiler M H. Landau levels in the valence band of tellurium. Solid State Commun, 1970, 8, 1017
[23] Thanh D. Effective mass approximation for acceptors in tellurium. Solid State Commun, 1971, 9, 631
[24] Shinno H, Yoshizaki R, Tanaka S, et al. Conduction band structure of tellurium. J Phys Soc Jpn, 1973, 35, 525
[25] Enderlein R, Hache A. Valence and conduction band structure and infrared optical properties of tellurium in the presence of pressure. Phys Status Solidi B, 1973, 60, 739
[26] Agapito L A, Kioussis N, Goddard W A, et al. Novel family of chiral-based topological insulators: Elemental tellurium under strain. Phys Rev Lett, 2013, 110, 176401
[27] Lin S Q, Li W, Chen Z W, et al. Tellurium as a high-performance elemental thermoelectric. Nat Commun, 2016, 7, 10287
[28] Akahama Y, Okawa N, Sugimoto T, et al. Coexistence of a metastable double hcp phase in bcc–fcc structure transition of Te under high pressure. Jpn J Appl Phys, 2018, 57, 025601
[29] Tanaka Y, Collins S P, Lovesey S W, et al. Determination of the absolute chirality of tellurium using resonant diffraction with circularly polarized X-rays. J Phys Condens Matter, 2010, 22, 122201
[30] Hirayama M, Okugawa R, Ishibashi S, et al. Weyl node and spin texture in trigonal tellurium and selenium. Phys Rev Lett, 2015, 114, 206401
[31] Nakayama K, Kuno M, Yamauchi K, et al. Band splitting and Weyl nodes in trigonal tellurium studied by angle-resolved photoemission spectroscopy and density functional theory. Phys Rev B, 2017, 95, 125204
[32] Sakano M, Hirayama M, Takahashi T, et al. Radial spin texture in elemental tellurium with chiral crystal structure. Phys Rev Lett, 2020, 124, 136404
[33] Dong Z Y, Ma Y H. Atomic-level handedness determination of chiral crystals using aberration-corrected scanning transmission electron microscopy. Nat Commun, 2020, 11, 1588
[34] Donohue J. The structure of the elements. New York: John Wiley & Sons, 1974
[35] Kabalkina S S, Vereshchagin L F, Shulenin B M. Phase transitions in tellurium at high pressures. J Exp Theor Phys, 1964, 45, 2073
[36] Jamieson J C, McWhan D B. Crystal structure of tellurium at high pressures. J Chem Phys, 1965, 43, 1149
[37] Aoki K, Shimomura O, Minomura S. Crystal structure of the high-pressure phase of tellurium. J Phys Soc Jpn, 1980, 48, 551
[38] Akahama Y, Kobayashi M, Kawamura H. Pressure-induced superconductivity and phase transition in selenium and tellurium. Solid State Commun, 1992, 84, 803
[39] Wang Y C, Lv J, Zhu L, et al. Crystal structure prediction via particle-swarm optimization. Phys Rev B, 2010, 82, 094116
[40] Reed E J. Two-dimensional tellurium. Nature, 2017, 552, 40
[41] Zhu Z L. First-principles study of new two-dimensional materials design and properties tuning. PhD Dissertation, Zhengzhou University, 2017 (in Chinese)
[42] Liu D, Lin X Q, Tománek D. Microscopic mechanism of the helix-to-layer transformation in elemental group VI solids. Nano Lett, 2018, 18, 4908
[43] Xian L D, Pérez Paz A, Bianco E, et al. Square selenene and tellurene: Novel group VI elemental 2D materials with nontrivial topological properties. 2D Mater, 2017, 4, 041003
[44] Zhang W, Wu Q S, Yazyev O V, et al. Topological phase trans-

itions driven by strain in monolayer tellurium. Phys Rev B, 2018, 98, 115411
[45] Paulauskas T, Sen F G, Sun C, et al. Stabilization of a monolayer tellurene phase at CdTe interfaces. Nanoscale, 2019, 11, 14698
[46] Qi L J, Han J, Gao W, et al. Monolayer tellurenyne assembled with helical telluryne: Structure and transport properties. Nanoscale, 2019, 11, 4053
[47] Wang Y, Xiao C C, Chen M G, et al. Two-dimensional ferroelectricity and switchable spin-textures in ultra-thin elemental Te multilayers. Mater Horiz, 2018, 5, 521
[48] Wang C, Zhou X Y, Qiao J S, et al. Charge-governed phase manipulation of few-layer tellurium. Nanoscale, 2018, 10, 22263
[49] Xiang Y, Gao S J, Xu R G, et al. Phase transition in two-dimensional tellurene under mechanical strain modulation. Nano Energy, 2019, 58, 202
[50] Wu B Z, Liu X H, Yin J R, et al. Bulk β-Te to few layered β-tellurenes: Indirect to direct band-gap transitions showing semiconducting property. Mater Res Express, 2017, 4, 095902
[51] Zhu Y J, Hu X L, Wang W W. Poly(vinylpyrrolidone): a new reductant for preparation of tellurium nanorods, nanowires, and tubes from TeO_2. Nanotechnology, 2006, 17, 645
[52] Qian H S, Yu S H, Gong J Y, et al. High-quality luminescent tellurium nanowires of several nanometers in diameter and high aspect ratio synthesized by a poly (vinyl pyrrolidone)-assisted hydrothermal process. Langmuir, 2006, 22, 3830
[53] Mo M, Zeng J, Liu X, et al. Controlled hydrothermal synthesis of thin single-crystal tellurium nanobelts and nanotubes. Adv Mater, 2002, 14, 1658
[54] Wang Q S, Safdar M, Xu K, et al. Van der Waals epitaxy and photoresponse of hexagonal tellurium nanoplates on flexible mica sheets. ACS Nano, 2014, 8, 7497
[55] Wu W Z, Qiu G, Wang Y X, et al. Tellurene: its physical properties, scalable nanomanufacturing, and device applications. Chem Soc Rev, 2018, 47, 7203
[56] Churchill H O H, Salamo G J, Yu S Q, et al. Toward single atom chains with exfoliated tellurium. Nanoscale Res Lett, 2017, 12, 1
[57] Lin Y, Wu Y, Wang R, et al. Two-dimensional tellurium nanosheets for photoacoustic imaging-guided photodynamic therapy. Chem Commun, 2018, 54, 8579
[58] Xie Z J, Xing C Y, Huang W C, et al. Ultrathin 2D nonlayered tellurium nanosheets: Facile liquid-phase exfoliation, characterization, and photoresponse with high performance and enhanced stability. Adv Funct Mater, 2018, 28, 1705833
[59] Zhang F, Liu G W, Wang Z P, et al. Broadband nonlinear absorption properties of two-dimensional hexagonal tellurene nanosheets. Nanoscale, 2019, 11, 17058
[60] Guo J, Zhao J L, Huang D Z, et al. Two-dimensional tellurium-polymer membrane for ultrafast photonics. Nanoscale, 2019, 11, 6235
[61] Wang Y, Qiu G, Wang R, et al. Field-effect transistors made from solution-grown two-dimensional tellurene. Nat Electron, 2018, 1, 228
[62] Wang Y X, de Souza Borges Ferreira R, Wang R X, et al. Data-driven and probabilistic learning of the process-structure-property relationship in solution-grown tellurene for optimized nanomanufacturing of high-performance nanoelectronics. Nano Energy, 2019, 57, 480
[63] Chen Y S, Ding J, He X M, et al. Synthesis of tellurium nanosheet for use in matrix assisted laser desorption/ionization time-of-flight mass spectrometry of small molecules. Microchim Acta, 2018, 185, 1
[64] Gao M, Wang X W, Hong Y Z, et al. One-pot hydrothermal synthesis of thin tellurene nanosheet and its formation mechanism. J Nanomater, 2019, 2019, 1
[65] Huang X C, Guan J Q, Lin Z J, et al. Epitaxial growth and band structure of Te film on graphene. Nano Lett, 2017, 17, 4619
[66] Chen J L, Dai Y W, Ma Y Q, et al. Ultrathin β-tellurium layers grown on highly oriented pyrolytic graphite by molecular-beam epitaxy. Nanoscale, 2017, 9, 15945
[67] Khatun S, Banerjee A, Pal A J. Nonlayered tellurene as an elemental 2D topological insulator: Experimental evidence from scanning tunneling spectroscopy. Nanoscale, 2019, 11, 3591
[68] Yang S, Chen B, Qin Y, et al. Highly crystalline synthesis of tellurene sheets on two-dimensional surfaces: Control over helical chain direction of tellurene. Phys Rev Mater, 2018, 2, 104002
[69] Apte A, Bianco E, Krishnamoorthy A, et al. Polytypism in ultrathin tellurium. 2D Mater, 2018, 6, 015013
[70] Peng J, Pan Y, Yu Z, et al. Two-dimensional tellurium nanosheets exhibiting an anomalous switchable photoresponse with thickness dependence. Angew Chem Int Ed, 2018, 57, 13533
[71] Dong Y L, Zeng B W, Zhang X J, et al. Study on the strain-induced mechanical property modulations in monolayer Tellurene. J Appl Phys, 2019, 125, 064304
[72] Gao Z B, Tao F, Ren J. Unusually low thermal conductivity of atomically thin 2D tellurium. Nanoscale, 2018, 10, 12997
[73] Sharma S, Singh N, Schwingenschlögl U. Two-dimensional tellurene as excellent thermoelectric material. ACS Appl Energy Mater, 2018, 1, 1950
[74] Liu G, Gao Z B, Ren J. Anisotropic thermal expansion and thermodynamic properties of monolayer β-Te. Phys Rev B, 2019, 99, 195436
[75] Qiu G, Huang S Y, Segovia M, et al. Thermoelectric performance of 2D tellurium with accumulation contacts. Nano Lett, 2019, 19, 1955
[76] Lin C S, Cheng W D, Chai G L, et al. Thermoelectric properties of two-dimensional selenene and tellurene from group-VI elements. Phys Chem Chem Phys, 2018, 20, 24250
[77] Chang K, Liu J W, Lin H C, et al. Discovery of robust in-plane ferroelectricity in atomic-thick SnTe. Science, 2016, 353, 274
[78] Wang Y. Properties tuning of novel two-dimensional ferroic materials: A first-principles study. PhD Dissertation, Zhejiang University, 2018 (in Chinese)
[79] Cai X R, Ren Y Y, Wu M H, et al. Strain-induced phase transition and giant piezoelectricity in monolayer tellurene. Nanoscale, 2020, 12, 167
[80] Liu Y Y, Wu W Z, Goddard W A III. Tellurium: fast electrical and atomic transport along the weak interaction direction. J Am Chem Soc, 2018, 140, 550
[81] Yan J H, Pang H, Xu L, et al. Excellent device performance of sub-5-nm monolayer tellurene transistors. Adv Electron Mater, 2019, 5, 1900226
[82] Qiu G, Wang Y, Nie Y, et al. Quantum transport and band structure evolution under high magnetic field in few-layer tellurene. Nano Lett, 2018, 18, 5760
[83] Ren X L, Wang Y, Xie Z T, et al. Gate-tuned insulator–metal transition in electrolyte-gated transistors based on tellurene. Nano Lett, 2019, 19, 4738
[84] Li P K, Sau J D, Appelbaum I. Robust zero-energy bound states in a helical lattice. Phys Rev B, 2017, 96, 115446
[85] Li P K, Appelbaum I. Intrinsic two-dimensional states on the pristine surface of tellurium. Phys Rev B, 2018, 97, 201402
[86] Qiu G, Niu C, Wang Y, et al. Quantum hall effect of massive Weyl fermions in n-type tellurene films. arXiv: 1908.11495, 2019
[87] Niu C, Qiu G, Wang Y X, et al. Gate-tunable strong spin-orbit interaction in two-dimensional tellurium probed by weak antilocalization. Phys Rev B, 2020, 101, 205414
[88] Pan Y Y, Gao S Y, Yang L, et al. Dependence of excited-state properties of tellurium on dimensionality: From bulk to two dimensions to one dimensions. Phys Rev B, 2018, 98, 085135
[89] Deckoff-Jones S, Wang Y X, Lin H T, et al. Tellurene: A multifunctional material for midinfrared optoelectronics. ACS Photonics, 2019, 6, 1632

[90] Bao Q L, Zhang H, Wang Y, et al. Atomic-layer graphene as a saturable absorber for ultrafast pulsed lasers. Adv Funct Mater, 2009, 19, 3077

[91] Du J, Wang Q K, Jiang G B, et al. Ytterbium-doped fiber laser passively mode locked by few-layer molybdenum disulfide (MoS_2) saturable absorber functioned with evanescent field interaction. Sci Rep, 6346, 4, 6346

[92] Luo Z Q, Huang Y Z, Weng J, et al. 1.06 μm Q-switched ytterbium-doped fiber laser using few-layer topological insulator Bi_2Se_3 as a saturable absorber. Optics Express, 2013, 21, 29516

[93] Zhang S F, Zhang X Y, Wang H, et al. Size-dependent saturable absorption and mode-locking of dispersed black phosphorus nanosheets. Opt Mater Express, 2016, 6, 3159

[94] Wu L M, Huang W C, Wang Y Z, et al. 2D tellurium based high-performance all-optical nonlinear photonic devices. Adv Funct Mater, 2019, 29, 1806346

[95] Zhang W F, Wang G M, Xing F, et al. Passively Q-switched and mode-locked erbium-doped fiber lasers based on tellurene nanosheets as saturable absorber. Opt Express, 2020, 28, 14729

[96] Amani M, Tan C L, Zhang G, et al. Solution-synthesized high-mobility tellurium nanoflakes for short-wave infrared photodetectors. ACS Nano, 2018, 12, 7253

[97] Shen C F, Liu Y H, Wu J B, et al. Tellurene photodetector with high gain and wide bandwidth. ACS Nano, 2020, 14, 303

[98] Gao S Y, Sun C Q, Zhang X. Ultra-strong anisotropic photo-responsivity of bilayer tellurene: A quantum transport and time-domain first principle study. Nanophotonics, 2019, 9, 1931

[99] Berweger S, Qiu G, Wang Y X, et al. Imaging carrier inhomogeneities in ambipolar tellurene field effect transistors. Nano Lett, 2019, 19, 1289

[100] Wang J J, Guo Y R, Shen H, et al. A first-principles study of strain tuned optical properties in monolayer tellurium. RSC Adv, 2019, 9, 41703

[101] Ma H H, Hu W, Yang J L. Control of highly anisotropic electrical conductance of tellurene by strain-engineering. Nanoscale, 2019, 11, 21775

[102] Du Y C, Qiu G, Wang Y X, et al. One-dimensional van der waals material tellurium: Raman spectroscopy under strain and magneto-transport. Nano Lett, 2017, 17, 3965

[103] Wang X H, Wang D W, Yang A J, et al. Effects of adatom and gas molecule adsorption on the physical properties of tellurene: A first principles investigation. Phys Chem Chem Phys, 2018, 20, 4058

[104] Xu W P, Gan L Y, Wang R, et al. Surface adsorption and vacancy in tuning the properties of tellurene. ACS Appl Mater Interfaces, 2020, 12, 19110

[105] Wang D W, Yang A J, Lan T S, et al. Tellurene based chemical sensor. J Mater Chem A, 2019, 7, 26326

[106] Wines D, Kropp J A, Chaney G, et al. Electronic properties of bare and functionalized two-dimensional (2D) tellurene structures. Phys Chem Chem Phys, 2020, 22, 6727

[107] Liu D K, Gui Y G, Ji C, et al. Adsorption of SF_6 decomposition components over Pd (111): A density functional theory study. Appl Surf Sci, 2019, 465, 172

[108] Cui H P, Zheng K, Tao L Q, et al. Monolayer tellurene-based gas sensor to detect SF_6 decompositions: A first-principles study. IEEE Electron Device Lett, 2019, 40, 1522

[109] Liang Z F, Wang Y, Hua C Q, et al. Electronic structures of ultrathin tellurium nanoribbons. Nanoscale, 2019, 11, 14134

[110] Lv Y, Liu Y, Qin W J, et al. Prediction of stable and high-performance charge transport in zigzag tellurene nanoribbons. IEEE Trans Electron Devices, 2019, 66, 2365

[111] Li H, Wu K, Yang S J, et al. Anomalous phase transition behavior in hydrothermal grown layered tellurene. Nanoscale, 2019, 11, 20245

[112] Gao S J, Wang Y X, Wang R X, et al. Piezotronic effect in 1D van der Waals solid of elemental tellurium nanobelt for smart adaptive electronics. Semicond Sci Technol, 2017, 32, 104004

[113] Kang J, Tongay S, Zhou J, et al. Band offsets and heterostructures of two-dimensional semiconductors. Appl Phys Lett, 2013, 102, 012111

[114] Liao J M, Sa B S, Zhou J, et al. Design of high-efficiency visible-light photocatalysts for water splitting: MoS_2/AlN(GaN) heterostructures. J Phys Chem C, 2014, 118, 17594

[115] Wu Q K, Jang S K, Park S, et al. *In situ* synthesis of a large area boron nitride/graphene monolayer/boron nitride film by chemical vapor deposition. Nanoscale, 2015, 7, 7574

[116] Zhang X R, Meng Z S, Rao D W, et al. Efficient band structure tuning, charge separation, and visible-light response in ZrS_2-based van der Waals heterostructures. Energy Environ Sci, 2016, 9, 841

[117] Si C, Lin Z Z, Zhou J, et al. Controllable Schottky barrier in GaSe/graphene heterostructure: The role of interface dipole. 2D Mater, 2016, 4, 015027

[118] Wu K, Ma H H, Gao Y Z, et al. Highly-efficient heterojunction solar cells based on two-dimensional tellurene and transition metal dichalcogenides. J Mater Chem A, 2019, 7, 7430

[119] Cai X L, Jia X T, Liu Y J, et al. Enhanced carrier mobility and tunable electronic properties in α-tellurene monolayer via an α-tellurene and h-BN heterostructure. Phys Chem Chem Phys, 2020, 22, 6434

[120] Qin X M, Hu W, Yang J L. Tunable Schottky and Ohmic contacts in graphene and tellurene van der Waals heterostructures. Phys Chem Chem Phys, 2019, 21, 23611

[121] Yan J H, Zhang X Y, Pan Y Y, et al. Monolayer tellurene–metal contacts. J Mater Chem C, 2018, 6, 6153

[122] Pang H, Yan J H, Yang J, et al. Bilayer tellurene–metal interfaces. J Semicond, 2019, 40, 062003

[123] Zhang W L, Chang D H, Gao Q, et al. Interlayer coupling and external electric field tunable electronic properties of a 2D type-I α-tellurene/MoS_2 heterostructure. J Mater Chem C, 2018, 6, 10256

[124] Ma Z, Wang Y S, Wei Y T, et al. A type-II C_2N/α-Te van der Waals heterojunction with improved optical properties by external perturbation. Phys Chem Chem Phys, 2019, 21, 21753

[125] Obeid M M. Tuning the electronic and optical properties of type-I PbI_2/α-tellurene van der Waals heterostructure via biaxial strain and external electric field. Appl Surf Sci, 2020, 508, 144824

[126] Yu W Y, Li S F, Cai X L, et al. Ferromagnetic half-metal properties of two dimensional vertical tellurene/VS_2 heterostructure: A first-principles study. Comput Mater Sci, 2020, 171, 109215

[127] Zhuang H L, Hennig R G. Stability and magnetism of strongly correlated single-layerVS_2. Phys Rev B, 2016, 93, 054429

[128] Fuh H R, Chang C R, Wang Y K, et al. Newtype single-layer magnetic semiconductor in transition-metal dichalcogenides VX_2 (X = S, Se and Te). Sci Rep, 2016, 6, 32625